JACS
JOURNAL OF THE AMERICAN CHEMICAL SOCIETY
Article
pubs.acs.org/JACS

Transformation from Kinetically into Thermodynamically Controlled Self-Organization of Complex Helical Columns with 3D Periodicity Assembled from Dendronized Perylene Bisimides

Virgil Percec,*[,†] Hao-Jan Sun,[†,‡] Pawaret Leowanawat,[†] Mihai Peterca,[†,‡] Robert Graf,[§] Hans W. Spiess,[§] Xiangbing Zeng,[∥] Goran Ungar,[∥,#] and Paul A. Heiney[‡]

[†]Roy & Diana Vagelos Laboratories, Department of Chemistry, University of Pennsylvania, Philadelphia, Pennsylvania 19104-6323, United States

[‡]Department of Physics and Astronomy, University of Pennsylvania, Philadelphia, Pennsylvania 19104-6396, United States

[§]Max-Planck Institute for Polymer Research, 55128 Mainz, Germany

[∥]Department of Materials Science and Engineering, University of Sheffield, Sheffield S1 3JD, United Kingdom

[#]WCU C2E2, School of Chemical and Biological Engineering, Seoul National University, Seoul 151-744, Korea

Supporting Information

ABSTRACT: The dendronized perylene 3,4:9,10-tetracarboxylic acid bisimide (PBI), (3,4,5)12G1-1-PBI, was reported by our laboratory to self-assemble into complex helical columns containing dimers of dendronized PBI with one molecule in each stratum, with different intra- and interdimer rotation angles but identical intra- and interdimer distance of 3.5 Å, exhibiting a four-strata 2_1 helical repeat. A thermodynamically controlled 2D columnar hexagonal phase with short-range intracolumnar order represents the thermodynamic product at high temperature, while a kinetically controlled monoclinic columnar array with 3D periodicity is the thermodynamic product at low temperature. With heating and cooling rates higher than 10 °C/min to 1 °C/min, at low temperature the 2D columnar periodic array is the kinetic product for this dendronized PBI. Here the synthesis and structural analysis of a library of (3,4,5)*n*G1-*m*-PBI with n = 12 to 6 and m = 1 are reported. A combination of differential scanning calorimetry, X-ray diffraction on powder and orientated fibers, including pattern simulation and electron density map reconstruction, and solid-state NMR, all as a function of temperature and heating and cooling rate, was employed for their structural analysis. It was discovered that at low temperature the as-prepared n = 12 to 10 exhibit a 3D layered array that transforms irreversibly into columnar periodicities during heating and cooling. Also the kinetically controlled 3D columnar phase of n = 12 becomes thermodynamically controlled for n = 10, 9, 8, 7, and 6. This unprecedented transformation is expected to facilitate the design of functions from dendronized PBI and other self-assembling building blocks.

INTRODUCTION

Perylene 3,4:9,10-tetracarboxylic acid bisimides (PBIs) have been elaborated into self-assembling building blocks employed in the design of complex systems[1] and supra-[2] and macromolecular[3] assemblies that impact fields such as dyes and pigments,[4] semiconductors, transistors, light-emitting diodes, solar cells,[2,3] artificial photosynthesis, life science and biology,[5] and xerographic receptors.[6] This extraordinary diversity of functions is facilitated by the excellent thermal and photochemical stability, the ability to functionalize the imide and bay positions, and the polymorphism[4d−f] exhibited by PBIs in their ordered states.

PBIs dendronized at bay,[7] imide,[8] or both positions with self-assembling dendrons have emerged as a powerful class of building blocks used to provide most of the functions and applications mentioned above. Both in solution and in solid state, the functions of these complex assemblies are determined by their two- and three-dimensional (2D and 3D) periodic or quasiperiodic structure.[9] Due to the polymorphic arrangement of supramolecular structures obtained from PBI building blocks in their 2D and 3D periodic and quasiperiodic arrays, their assembly is determined by a delicate combination of kinetically and thermodynamically controlled pathways and mechanisms.[10] Our laboratory is using the generational and deconstruction library approaches[11] to discover supramolecular organizations[12] and predict the primary structure required to self-organize a certain functional 3D periodic array. This library approach[11,12] is currently applied to PBI dendronized at the imide positions with the self-assembling dendrons (3,4,5)*n*G1-*m*-PBI,[13] where n is the number of carbons in their *n*-alkyls and m is the numbers of methylenic units connecting the dendron

Received: January 19, 2013
Published: February 14, 2013

   dx.doi.org/10.1021/ja400639q | J. Am. Chem. Soc. 2013, 135, 4129−4148

to the imide group (Scheme 1). This approach led to the discovery of a diversity of unprecedented helical columnar

Scheme 1. Schematic of the Self-Assembly of Dendronized PBIs, (3,4,5)*n*G1-*m*-PBI

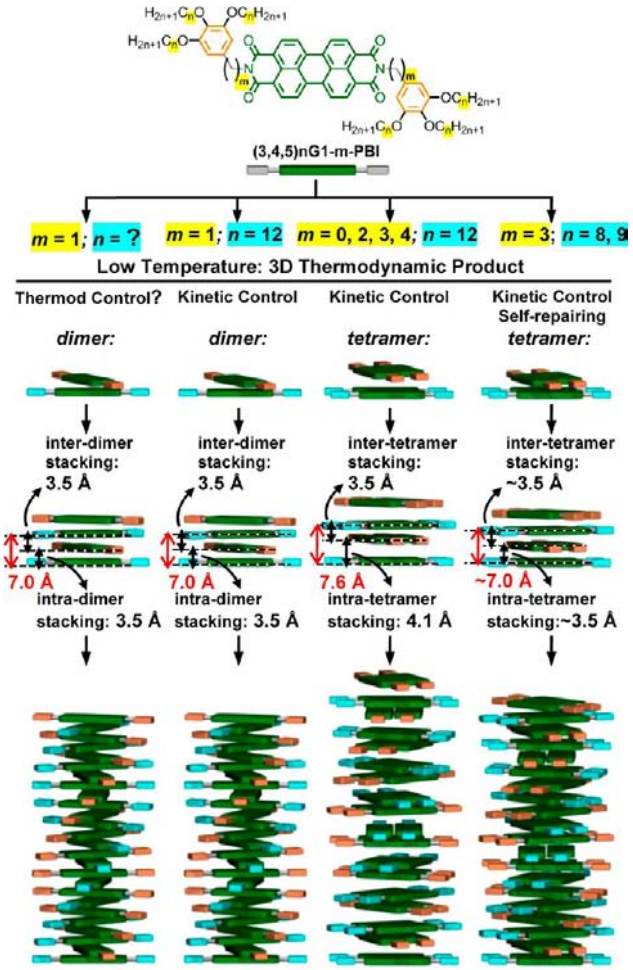

arrangements that are briefly outlined in Scheme 1.[13] The compounds with m = 0, 2, 3, 4 and n = 12 self-assemble during heating and cooling into helical columns containing tetramers of PBI as basic repeat units (see right two columns in Scheme 1). These tetramers consist of a pair of two molecules arranged side-by-side and another pair in the next stratum of the column turned upside-down and rotated around the column axis. The intra- and intertetramer rotation angles and stacking distances are different.[13a] The helical columns generated from m = 0, 2, 3, 4 and n = 12 self-organize at high temperature via a thermodynamically controlled mechanism in a 2D hexagonal columnar phase with short-range intracolumnar order, while at low temperature they assemble in 3D columnar arrays via a kinetically controlled process. Screening through a library with m = 3 and n = 14 to 4[13b] led to the discovery of a kinetically controlled self-repairing process that produced a single intra- and intertetramer distance of 3.5 Å for the helical columns assembled from m = 3, n = 8, 9 (right column in Scheme 1). In contrast, for m = 1, n = 12, the helical columns contain dimers of dendronized PBI with one molecule in each column stratum having different intra- and interdimer rotation angles and a 3.5 Å intra- and interdimer distance generating a four-strata 2_1 helical repeat.[13a] All PBIs face up in the first column and down in the second. This allows close and extended π-stacking that is expected to provide interesting charge carrier mobility and other properties, unlike the disruptive up−down alternation from the core of PBI building blocks with m = 0, 2, 3, 4 with n = 12.[13a,b] Due to the presence of the thermodynamically controlled 2D structure at high temperature and the kinetically controlled 3D array at low temperature, most of the time the 2D structure represents the kinetic product at low temperature and the 3D periodicity can be detected only by cooling at rates of 1 °C/min or less and by suitable annealing.[13a] The kinetically controlled self-organization of 3D structures is common.[14] However, kinetically controlled 3D structures are difficult to duplicate and, therefore, provide almost irreproducible pathways to discovery, elucidation of the mechanism, and proper manipulation of structures responsible for functions[14] of interest for technological applications such as organic electronics. A very fundamental question is illustrated in the left column of Scheme 1: Can the desirable self-organization of the 3D periodic four-strata 2_1 helical columnar structure be changed from a kinetically to a thermodynamically controlled process? And, if so, can it be accomplished via manipulation of the simplest parameters of the primary structure of the dendronized PBI (left column in Scheme 1)?

Here we report the synthesis and structural analysis of a library of (3,4,5)*n*G1-1-PBI with n = 12, 11, 10, 9, 8, 7, 6. The analysis of this library led to the discovery of dendronized PBIs that transformed the kinetically controlled self-organization of the 3D crystalline structures containing helical columns of n = 12 and 11 into thermodynamically controlled 3D crystalline structures for n = 10, 9, 8. It also led to the discovery that the n = 12 to 10 PBIs as-prepared from solution self-organize in a 3D layered periodic array that is not obtained during subsequent heating and cooling scans when only 3D and 2D columnar periodic arrays form. At high temperature all PBIs with n = 12 to 8 display also a 2D hexagonal columnar lattice with short-range intracolumnar order. Compounds with n = 7, 6 exhibit only 3D crystalline structures that are also thermodynamically controlled. We expect that the discovery of the thermodynamically controlled self-organization of 3D columnar structures reported here, that we name *TCC soft crystals*, will impact the design of functions and the development of technological application for many fields, including supramolecular organic electronics.

RESULTS AND DISCUSSION

Synthesis of Dendronized PBI (3,4,5)*n*G1-1-PBI. The synthesis of twin-dendronized[13,15] (3,4,5)*n*G1-1-PBIs with n = 12, 11, 10, 9, 8, 7, 6 is outlined in Scheme 2. In the first step, methyl 3,4,5-trihydroxybenzoate (**1**) was etherified with benzyl chloride in degassed dimethylformamide (DMF) in the presence of K_2CO_3 at 75 °C to produce methyl 3,4,5-tris(benzyloxy)benzoate (**2**) in 92% yield after passing its CH_2Cl_2 solution through a short column of basic Al_2O_3 followed by precipitation into MeOH. Reduction of **2** with $LiAlH_4$ yielded (3,4,5-tris(benzyloxy)phenyl)methanol (**3**) in 99% yield. Bromination of **3** with NBS/PPh_3 in THF produced **4** (88% yield). The nucleophilic displacement of **4** with potassium phthalimide in dry DMF produced **5** in 95% yield which after hydrogenolysis with Pd/C in MeOH/CH_2Cl_2 (1/2) at 24 °C for 12 h yielded **6** (100% yield). Compound **6** was etherified with the *n*-alkyl bromides containing 12, 11, 10, 9, 8, 7, and 6 carbons to produce the corresponding **7a**−**7g** in 65−91% yields. Treatment of the phthalimide derivatives **7a**−**7g**

dx.doi.org/10.1021/ja400639q | J. Am. Chem. Soc. 2013, 135, 4129−4148

Scheme 2. Synthesis of Dendronized PBIs, (3,4,5)*n*G1-1-PBI, with *n* = 12, 11, 10, 9, 8, 7, 6[a]

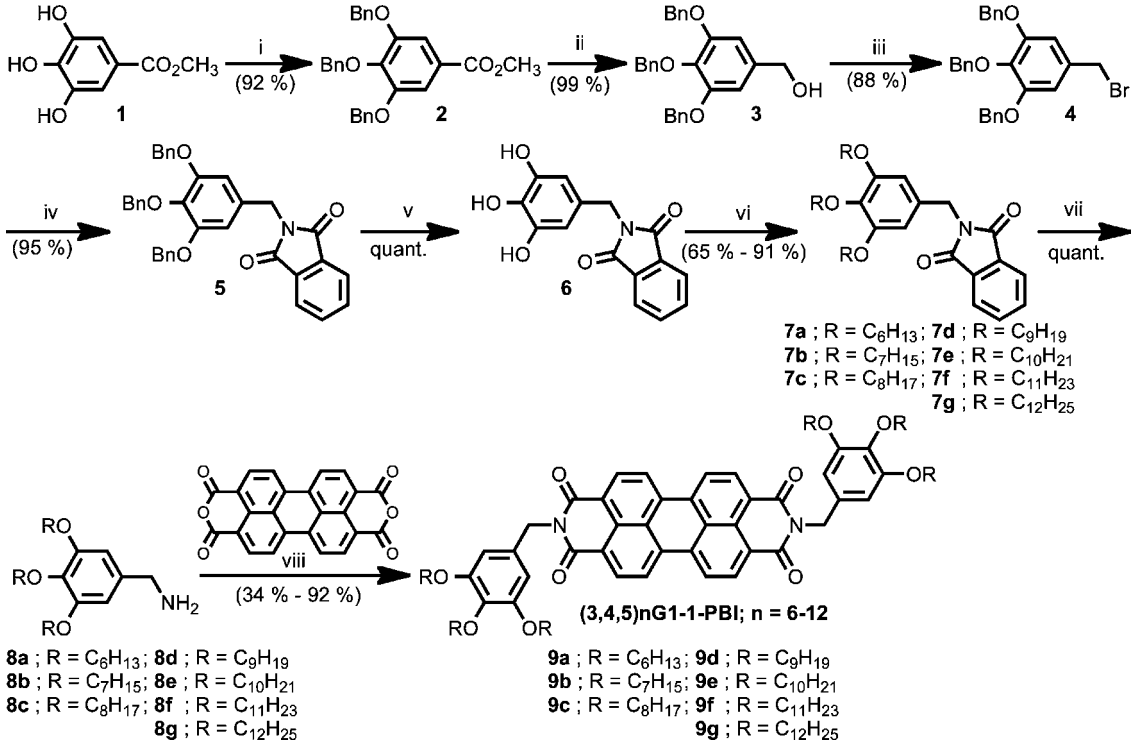

[a]Reagents and conditions: (i) BnCl, K_2CO_3, 75 °C; (ii) $LiAlH_4$, THF; (iii) PPh_3, NBS, THF; (iv) potassium phthalimide, DMF, 70 °C; (v) H_2, Pd/C, MeOH−CH_2Cl_2; (vi) $C_nH_{2n+1}Br$, K_2CO_3, DMF; (vii) $H_2NNH_2.H_2O$, EtOH, reflux; (viii) $Zn(OAc)_2$, quinoline, 180 °C.

with 64% hydrazine hydrate in absolute EtOH at reflux for 12 h produced compounds **8a−8g** in quantitative yield. Imidization of perylene-3,4:9,10-tetracarboxylic dianhydride with the amines **8a−8g** was performed in quinoline at 180 °C (4−6 h) in the presence of $Zn(OAc)_2{\cdot}H_2O$ to produce **9a−9g** in 34−92% yield after purification by column chromatography (SiO_2, 0 − 2% acetone in CH_2Cl_2), followed by precipitation in methanol from concentrated CH_2Cl_2 solution. ^1H and ^{13}C NMR, MALDI-TOF, and HPLC demonstrated a purity higher than 99% for all (3,4,5)*n*G1-1-PBI (**9a−9g**) (Supporting Information).

Analysis of the Supramolecular Assemblies and Their Periodic Arrays by a Combination of Differential Scanning Calorimetry and X-ray Diffraction. This analysis requires a comparative inspection of the differential scanning calorimetry (DSC) results obtained at 10 °C/min (Figure 1) and 1 °C/min (Figure 2). Identification of the 2D columnar hexagonal phase with short-range intracolumnar order, Φ_h^{io}, the 3D columnar centered orthorhombic, $\Phi_{c\text{-}o}^{k}$, two different columnar monoclinic lattices, Φ_m^{k1} and Φ_m^{k2}, and a columnar monoclinic superlattice, $\Phi_m^{k\text{-}SL}$, reported in Figures 1 and 2 was accomplished by a combination of X-ray diffraction (XRD) experiments performed at small and wide angles on powder and oriented fibers.[12,13] Note that the term "centered orthorhombic" is used here to distinguish this phase from the "simple orthorhombic" reported previously.[13]

Data from Figures 1 and 2 are summarized in Table 1. Thermodynamically controlled phase transitions are usually observed for 2D liquid crystalline periodic arrays.[14] The transition temperatures from 2D to isotropic liquid and from isotropic liquid to 2D are almost identical, regardless of the heating and cooling rate of the DSC, and exhibit only a small degree of supercooling that usually is less than 10 °C. The enthalpy changes associated with thermodynamically controlled phase transitions display also a very small dependence on rate and on the heating and cooling history of the sample. By considering these rules, a brief inspection of the DSC traces from Figures 1 and 2 demonstrates that the temperatures of the transitions from Φ_h^{io} to isotropic liquid (i) and from i to Φ_h^{io} for compounds with *n* = 12, 11, 10, 9, and 8, and their enthalpy changes are almost identical, regardless of whether they are determined from heating or cooling scans performed at 10 or 1 °C/min. Regardless of rate, for *n* = 12 to 8, the temperature that corresponds to the i-to-Φ_h^{io} transition determined on cooling is only 1 °C lower than that for the Φ_h^{io}-to-i transition determined on heating. Therefore, at high temperature the supramolecular columns forming the Φ_h^{io} periodic array represent the thermodynamic product of the self-assembly process, and their formation is thermodynamically controlled.

In the case of *n* = 12, 11, and 10, the DSC combined with XRD data obtained from the first heating scans recorded with 10 °C/min (Figure 1) and 1 °C/min (Figure 2) demonstrate the formation of some layered 3D periodic arrays that are not reformed during the subsequent heating and cooling scans. The as-prepared sample used during the first heating scan was obtained by the slow evaporation of a CH_2Cl_2 solution, which generally allows the formation of the phase that is closest to equilibrium. A closer inspection of the cooling and second heating scans obtained with 10 and 1 °C/min for *n* = 12 shows substantial differences for the 3D periodic arrays observed at lower temperature than the Φ_h^{io}. After cooling from the isotropic liquid at 10 °C/min, only the Φ_h^{io} is obtained, judged by the absence of any endotherm with a significant enthalpy on second heating (Figure 1). However, after cooling at 1 °C/min, a 3D phase which undergoes a transition to Φ_h^{io} at 33 °C and has a very small enthalpy change is observed (Figure 2).

dx.doi.org/10.1021/ja400639q | J. Am. Chem. Soc. 2013, 135, 4129−4148

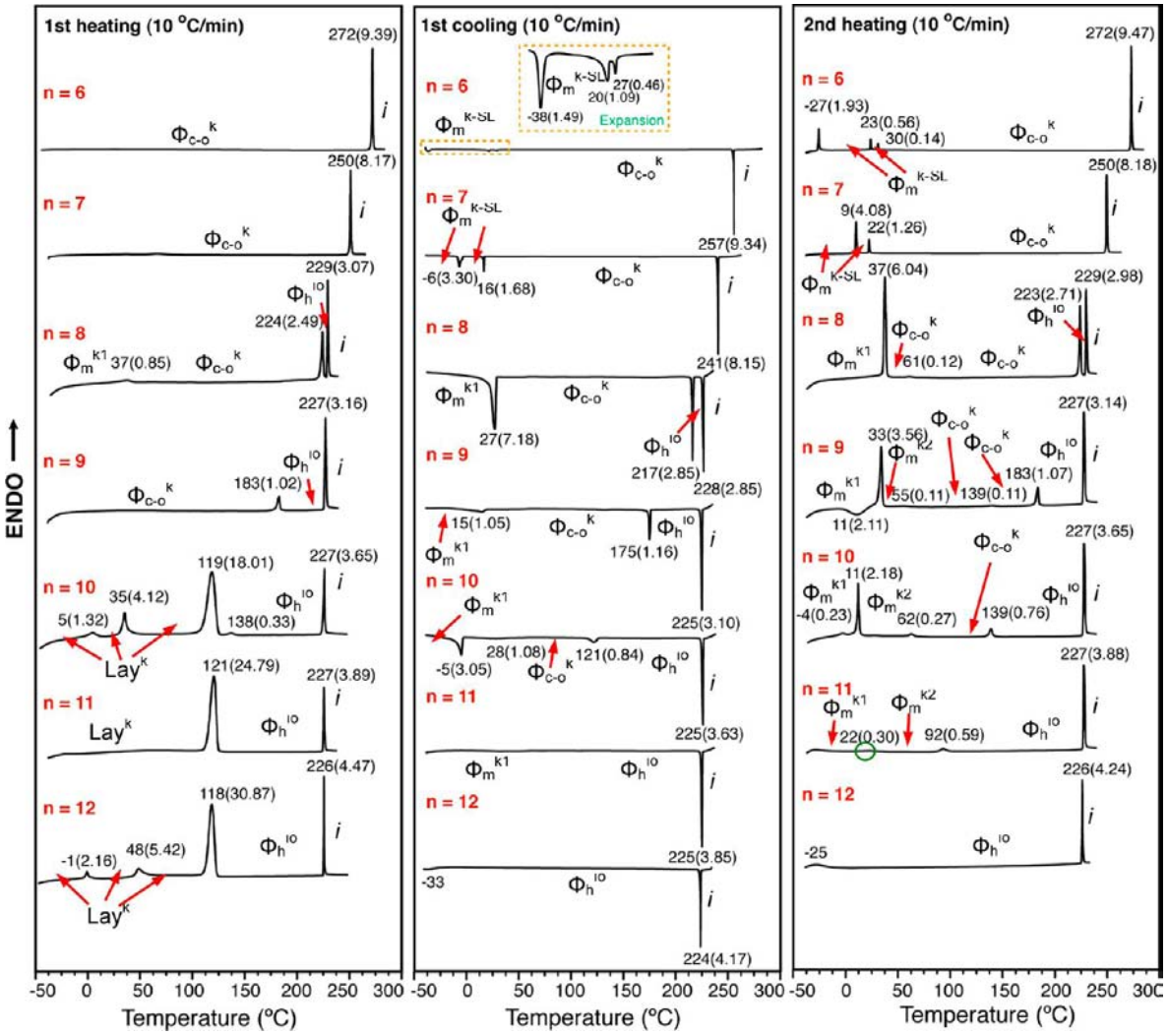

Figure 1. DSC traces collected from (3,4,5)*n*G1-1-PBI with n = 6 to 12 at heating and cooling rates of 10 °C/min. Phases, transition temperatures, and associated enthalpy changes (in parentheses, in kcal/mol) are indicated. The green circles show the transitions dependent on rate.

Annealing at 24 °C for 1 month increases the transition enthalpy and temperature (to 39 °C); see inset on second heating scan for n = 12 in Figure 2. DSC heating scans for n = 12 after annealing at 24 °C for various periods of time are shown in Figure 3.

For n = 12, the 3D phase is the thermodynamic product at low temperature. However, the formation of the 3D phase is strongly dependent on rate and, therefore, is kinetically controlled. Since n = 12 exhibits a 2D thermodynamic product at high temperature (Φ_h^{io}) that is thermodynamically controlled (i.e., independent of rate), with a cooling rate of 10 °C/min we observed at low temperature the Φ_h^{io} phase that this time, in this range of temperature, is the kinetic product. However, for most functions and applications of supramolecular periodic array, the 3D thermodynamic product that is kinetically controlled is the desired structure. Therefore, it is of great interest to discover the simplest possible changes to the chemical structure of the dendronized PBI that may allow the transformation of the 3D thermodynamic product from being kinetically controlled to thermodynamically controlled. In addition, it would also be very important if the temperature of the 3D thermodynamically controlled product could be engineered to be in the proper range of interest for potential technological applications.

Inspection of the DSC data for n = 11 by following the same principles as those used in the case of n = 12 starts to show a promising change. At both 10 and 1 °C/min, cooling and second heating scans show the formation of the 3D Φ_m^{k1} monoclinic phase that was not observed for n = 12. However, the melting of Φ_m^{k1} at 35 °C with 1 °C/min on heating, and the formation of Φ_m^{k1} at 8 °C with the same rate on cooling, show a difference of 27 °C. For n = 11, no Φ_h^{io} is observed as a kinetic product at low temperature (Figures 1 and 2 compare n = 12 with n = 11), but the formation of the 3D Φ_m^{k1} phase near room temperature for n = 11 remains kinetically controlled.

Compounds with n = 10, 9, and 8 provide an unexpected and remarkable result. The temperature transition from 2D to 3D and from 3D to 2D phases and their associated enthalpy changes are very little dependent on the heating and cooling rate and on the heating and cooling temperature from which they are collected (compare Figures 1 and 2). To our knowledge, these compounds provide the first examples of 3D periodic arrays self-organized from complex helical columns that behave just like the 2D periodic arrays; i.e., they are thermodynamically controlled. It is also extremely rewarding

dx.doi.org/10.1021/ja400639q | J. Am. Chem. Soc. 2013, 135, 4129−4148

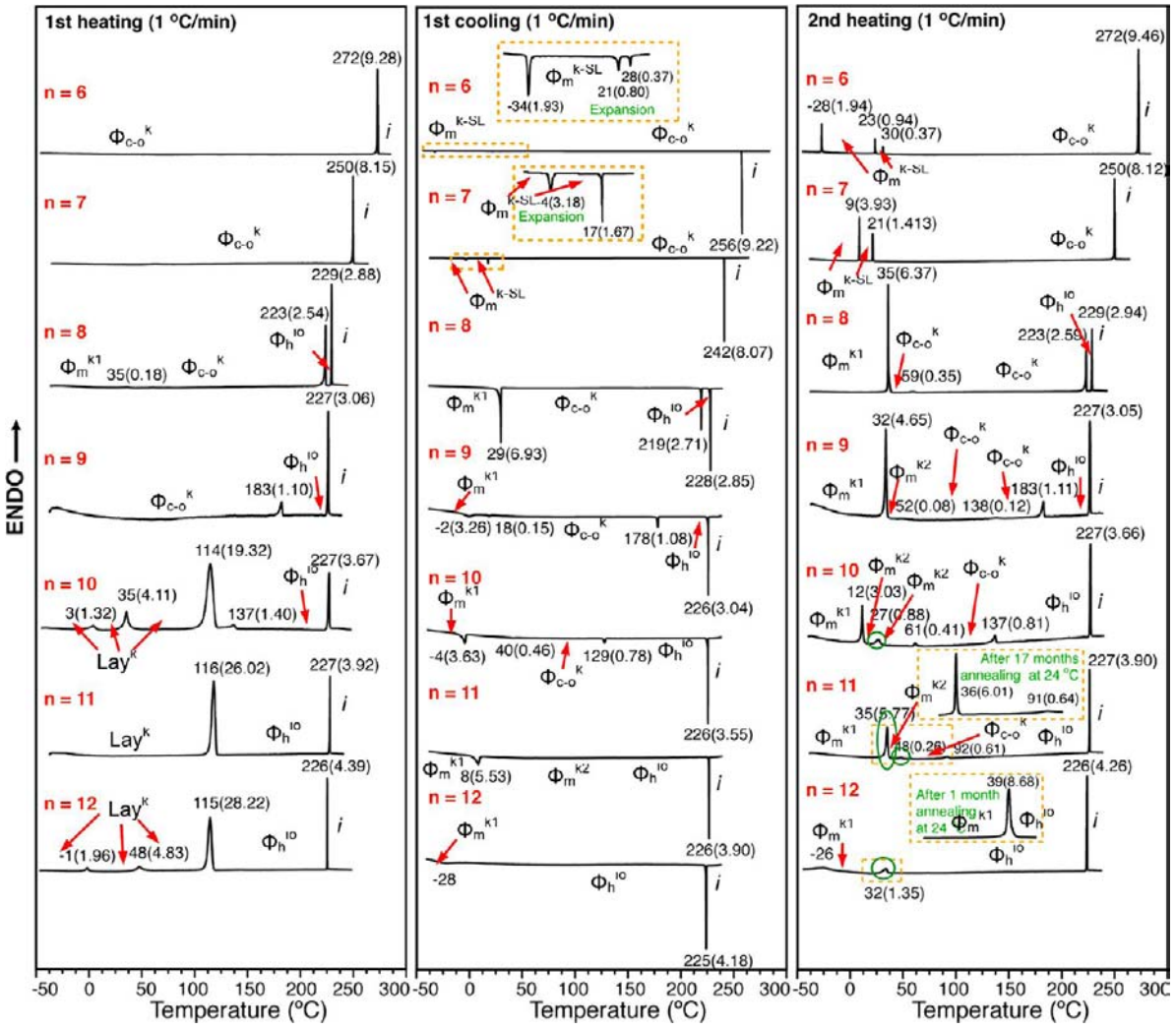

Figure 2. DSC traces collected from (3,4,5)*n*G1-1-PBI with n = 6 to 12 at heating and cooling rates of 1 °C/min. Phases, transition temperatures, and associated enthalpy changes (in parentheses, in kcal/mol) are indicated. The green circles show transitions dependent on rate.

that the 3D structures obtained from n = 10 are stable up to ~139 °C, the one for n = 9 up to ~183 °C, and the one for n = 8 up to ~223 °C (Figures 1, 2, and 4b). This range of temperature stability for the 3D thermodynamically controlled thermodynamic product is important for technological applications. Compounds with n = 7 and 6 do not exhibit the high-temperature 2D Φ_h^{io} phase. They self-organize only in 3D arrays that are all the thermodynamically controlled thermodynamic products. Figure 4a illustrates all 2D and 3D periodic arrays mentioned above.

Figure 4b summarizes the dependence of the structures of 2D and 3D periodic arrays self-organized for (3,4,5)*n*G1-1-PBI on n and temperature. For n = 12 and 11, the 3D periodic arrays of interest for electronic applications are stable up to 33 and 92 °C, respectively, and are kinetically controlled. For n = 10, 9, and 8, the 3D periodic arrays are stable up to 139, 183, and 223 °C, respectively, and are thermodynamically controlled. These assemblies also display a 2D Φ_h^{io} that is useful for the alignment and templated crystallization of their 3D periodic arrays. The compounds with n = 7 and 6 show a remarkable number of 3D phases that are all thermodynamically controlled. In addition, a layered crystalline structure was observed in n = 12, 11, and 10 during the first heating from the as-prepared sample obtained by slow evaporation of CH_2Cl_2 solution. This phase cannot be regenerated in the subsequent heating and cooling treatments. This phase is stable up to 118, 121, and 119 °C for n = 12, 11, and 10, respectively. Only for n = 12, this layered structure can also be obtained by precipitation from solution through addition of excess methanol.

A Brief Description of the 2D and 3D Periodic Arrays Self-Organized from Dendronized PBIs. Φ_h^{io} is a 2D lattice which possesses short-range order along the column axis. The $\Phi_{c\text{-}o}^{k}$ lattice has a column packing related to that observed in Φ_h^{io} except that the angle between neighboring columns is slightly deviated from 60° (Figure 4a). In addition there is long-range registry order between the supramolecular columns, and therefore $\Phi_{c\text{-}o}^{k}$ is a 3D crystal. The 3D $\Phi_m^{k\text{-}SL}$ phase observed in n = 7 and 6 at low temperature has its a-axis as the unique axis with the column tilted with respect to the ab plane, while other monoclinic phases found in this library have the c-axis as the unique axis. Each unit cell of the $\Phi_m^{k\text{-}SL}$ phase contains three subcells along the c-axis, and the length of the c-axis (~44.1 Å) is about 3 times longer than that for the $\Phi_{c\text{-}o}^{k}$ found at higher temperature (~14.7 Å). Notice that this phase does not form in the as-prepared samples from solution (absent during first heating) and develops only during cooling from high temperature. Φ_m^{k1}, with $P2_1/b$ symmerty, is the thermodynamic

dx.doi.org/10.1021/ja400639q | J. Am. Chem. Soc. 2013, 135, 4129−4148

Table 1. Transition Temperatures and Associated Enthalpy Changes of (3,4,5)*n*G1-1-PBI with *n* = 6 to 12 Determined by DSC and XRD

		thermal transition (°C) and corresponding enthalpy changes (kcal/mol)	
n	rate (°C/min)	heating[a]	cooling
6	10	$\Phi_{c\text{-}o}^{k}$ 272 (9.39) i $\Phi_{m}^{k\text{-}SL}$ −27 (1.93) $\Phi_{m}^{k\text{-}SL}$ 23 (0.56) $\Phi_{c\text{-}o}^{k}$ 272 (9.47) i	i 257 (−9.34) $\Phi_{c\text{-}o}^{k}$ 20 (−1.1) $\Phi_{m}^{k\text{-}SL}$ −38 (−1.49) $\Phi_{m}^{k\text{-}SL}$
	1	$\Phi_{c\text{-}o}^{k}$ 272 (9.28) i $\Phi_{m}^{k\text{-}SL}$ −28 (1.94) $\Phi_{m}^{k\text{-}SL}$ 23 (0.94) $\Phi_{c\text{-}o}^{k}$ 272 (9.46) i	i 258 (−9.2) $\Phi_{c\text{-}o}^{k}$ 21 (−0.80) $\Phi_{m}^{k\text{-}SL}$ −34 (−1.93) $\Phi_{m}^{k\text{-}SL}$
7	10	$\Phi_{c\text{-}o}^{k}$ 250 (8.17) i $\Phi_{m}^{k\text{-}SL}$ 9 (4.08) $\Phi_{m}^{k\text{-}SL}$ 22 (1.26) $\Phi_{c\text{-}o}^{k}$ 250 (8.18) i	i 241 (−8.15) $\Phi_{c\text{-}o}^{k}$ 16 (−1.68) $\Phi_{m}^{k\text{-}SL}$ −6 (−3.30) $\Phi_{m}^{k\text{-}SL}$
	1	$\Phi_{c\text{-}o}^{k}$ 250 (8.15) i $\Phi_{m}^{k\text{-}SL}$ 9 (3.93) $\Phi_{m}^{k\text{-}SL}$ 21 (1.41) $\Phi_{c\text{-}o}^{k}$ 250 (8.12) i	i 242 (−8.07) $\Phi_{c\text{-}o}^{k}$ 17 (−1.67) $\Phi_{m}^{k\text{-}SL}$ −4 (−3.18) $\Phi_{m}^{k\text{-}SL}$
8	10	Φ_{m}^{k1} 37 (0.85) $\Phi_{c\text{-}o}^{k}$ 224 (2.49) Φ_{h}^{io} 229 (3.07) i Φ_{m}^{k1} 37 (6.04) $\Phi_{c\text{-}o}^{k}$ 61 (0.12) $\Phi_{c\text{-}o}^{k}$ 223 (2.71) Φ_{h}^{io} 229 (2.98) i	i 228 (−2.85) Φ_{h}^{io} 217 (−2.85) $\Phi_{c\text{-}o}^{k}$ 27 (−7.18) Φ_{m}^{k1}
	1	Φ_{m}^{k1} 35 (0.18) $\Phi_{c\text{-}o}^{k}$ 223 (2.54) Φ_{h}^{io} 229 (2.88) i Φ_{m}^{k1} 35 (6.37) $\Phi_{c\text{-}o}^{k}$ 59 (0.35) $\Phi_{c\text{-}o}^{k}$ 223 (2.59) Φ_{h}^{io} 229 (2.94) i	i 228 (−2.85) Φ_{h}^{io} 219 (−2.71) $\Phi_{c\text{-}o}^{k}$ 29 (−6.93) Φ_{m}^{k1}
9	10	$\Phi_{c\text{-}o}^{k}$ 183 (1.02) Φ_{h}^{io} 227 (3.16) i Φ_{m}^{k1} 33 (3.56) Φ_{m}^{k2} 55 (0.11) $\Phi_{c\text{-}o}^{k}$ 139 (0.1) $\Phi_{c\text{-}o}^{k}$ 183 (1.07) Φ_{h}^{io} 227 (3.14) i	i 225 (−3.10) Φ_{h}^{io} 175 (−1.16) $\Phi_{c\text{-}o}^{k}$ 15 (−1.05) Φ_{m}^{k1}
	1	$\Phi_{c\text{-}o}^{k}$ 183 (1.10) Φ_{h}^{io} 227 (3.06) i Φ_{m}^{k1} 32 (4.65) Φ_{m}^{k2} 52 (0.08) $\Phi_{c\text{-}o}^{k}$ 138 (0.1) $\Phi_{c\text{-}o}^{k}$ 183 (1.11) Φ_{h}^{io} 227 (3.05) i	i 226 (−3.04) Φ_{h}^{io} 178 (−1.08) $\Phi_{c\text{-}o}^{k}$ 18 (−0.15) Φ_{m}^{k1}
10	10	Lay^{k} 5 (1.32) Lay^{k} 35 (4.12) Lay^{k} 119 (18.01) Φ_{h}^{io} 227 (3.65) i[c] Φ_{m}^{k1} 11 (2.18) Φ_{m}^{k2} 62 (0.27) $\Phi_{c\text{-}o}^{k}$ 139 (0.76) Φ_{h}^{io} 227 (3.65) i	i 225 (−3.63) Φ_{h}^{io} 121 (−0.84) $\Phi_{c\text{-}o}^{k}$ −5 (−3.05) Φ_{m}^{k1}
	1	Lay^{k} 3 (1.32) Lay^{k} 35 (4.11) Lay^{k} 114 (19.32) Φ_{h}^{io} 227 (3.67) i[c] Φ_{m}^{k1} 12 (3.03) Φ_{m}^{k2} 27 (0.88) Φ_{m}^{k2} 61 (0.41) $\Phi_{c\text{-}o}^{k}$ 137 (0.81) Φ_{h}^{io} 227 (3.66) i	i 226 (−3.55) Φ_{h}^{io} 129 (−0.78) $\Phi_{c\text{-}o}^{k}$ −4 (−3.63) Φ_{m}^{k1}
11	10	Lay^{k} 121 (24.79) Φ_{h}^{io} 227 (3.89) i Φ_{m}^{k1} 22 (0.30) Φ_{m}^{k2} 92 (0.59) Φ_{h}^{io} 227 (3.88) i	i 225 (−3.85) Φ_{h}^{io} —[b] Φ_{m}^{k1}
	1	Lay^{k} 116 (26.02) Φ_{h}^{io} 227 (3.92) i Φ_{m}^{k1} 35 (5.77) Φ_{m}^{k2} 48 (0.26) $\Phi_{c\text{-}o}^{k}$ 92 (0.61) Φ_{h}^{io} 227 (3.90) i	i 226 (−3.90) Φ_{h}^{io} —[b] $\Phi_{c\text{-}o}^{k}$ 8 (−5.53) Φ_{m}^{k1}
12	10	Lay^{k} −1 (2.16) Lay^{k} 48 (5.42) Lay^{k} 118 (30.87) Φ_{h}^{io} 226 (4.47) i[c] Φ_{h}^{io} 226 (4.24) i	i 224 (−4.17) Φ_{h}^{io}
	1	Lay^{k} −1 (1.96) Lay^{k} 48 (4.83) Lay^{k} 115 (28.22) Φ_{h}^{io} 226 (4.39) i[c] Φ_{m}^{k1} 32 (1.35) Φ_{h}^{io} 226 (4.26) i Φ_{m}^{k1} 39 (8.68) Φ_{h}^{io} 225 (4.21) i[d]	i 225 (−4.18) Φ_{h}^{io}

[a]Data from the first heating and cooling scans are on the first line, and data from the second heating are on the second line with rate indicated in second column. Phase notation: $\Phi_{c\text{-}o}^{k}$, columnar centered orthorhombic crystalline phase, $\Phi_{m}^{k\text{-}SL}$, columnar monoclinic crystalline superlattice; Φ_{m}^{k1}, Φ_{m}^{k2}, columnar monoclinic crystalline phase; Φ_{h}^{io}, 2D columnar hexagonal phase with intracolumnar order; Lay^{k}, layered monoclinic crystalline phase; i, isotropic. [b]This transition is observed by XRD. [c]Lattice parameters changed between the observed Lay^{k} phase (Table 2). [d]Second heating data collected after 1 month of annealing at 24 °C. Note: quantitative uncertainties are ±1 °C for thermal transition temperatures and ∼2% for the associated enthalpy changes reported in kcal/mol.

product at low temperature for *n* = 8, 9, 10, 11, 12. It contains two columns in one unit cell, and the cell symmetry translates the columns into alternative left- and right-handed helices along the *b*-axis. The Lay^{k} phase is found only in as-prepared sample from solution with *n* = 12, 11, and 10, where molecules pack in a monoclinic unit cell with the *b*-axis as the unique axis and cell symmetry of $P2_1$. In this structure, the PBI cores are tilted with respect to the *c*-axis and phase-separated from the alkyl chains. As will be discussed in more detail later, this phase possesses larger π−π stacking distance compared with other columnar 2D and 3D phases.

A first-order phase transition separates Φ_{m}^{k1} from Φ_{h}^{io} in *n* = 12 after annealing without going through other intermediary phases. In compounds with *n* = 11 to 8, Φ_{m}^{k2} and $\Phi_{c\text{-}o}^{k}$ were observed as intermediary phases between high-temperature 2D Φ_{h}^{io} and low-temeprature 3D Φ_{m}^{k1}. As shown in Figure 4a, Φ_{m}^{k2} has a column arrangement in the unit cell similar to that of $\Phi_{c\text{-}o}^{k}$, but the lattice is distorted in the *ab* plane. It seems that Φ_{m}^{k2} is more stable at lower temperature than $\Phi_{c\text{-}o}^{k}$; therefore, Φ_{m}^{k2} usually develops first, before $\Phi_{c\text{-}o}^{k}$, during heating from low temperature in the Φ_{m}^{k1} phase. Unlike in Φ_{m}^{k1} and Φ_{m}^{k2}, $\Phi_{m}^{k\text{-}SL}$ is distorted in the *bc* plane, where the *c*-axis is conventionally assigned as the column axis. This indicates that the columns in $\Phi_{m}^{k\text{-}SL}$ are tilted against the fiber direction when an orientated fiber is prepared. A similar trend was observed and reported previously in (3,4,5)9G1-3-PBI,[13b] where the low-temperature $\Phi_{c\text{-}o}^{k}$ was replaced by a more stable Φ_{m}^{k} as the thermodynamic product after annealing at 110 °C for 600 min in the Φ_{h}^{io}. All these compounds have isotropization temperatures above 225 °C, indicating an excellent range of thermal stability (Figure 4b) of their self-organized structures. The 2D Φ_{h}^{io} formed by compounds with *n* = 8 to 12 is the thermodynamic product at high temperature, but that for *n* = 12 is the kinetic product at low temperature, depending on the rate of cooling and on annealing. It is interesting to notice that the lower end of the temperature range of the Φ_{h}^{io} phase decreases with increasing *n*. This drop in the melting point of the 3D phases is consistent with the increasing transition entropy due to the increased conformational freedom of the longer peripheral alkyl chains. The XRD patterns of high-temperature 2D Φ_{h}^{io} phase obtained for *n* = 8 to 12 and low-temperature 3D crystalline phases obtained for *n* = 6 to 12 are summarized in Figures 5 and 6, respectively. The detailed structural evolution will be discussed in the following subsection.

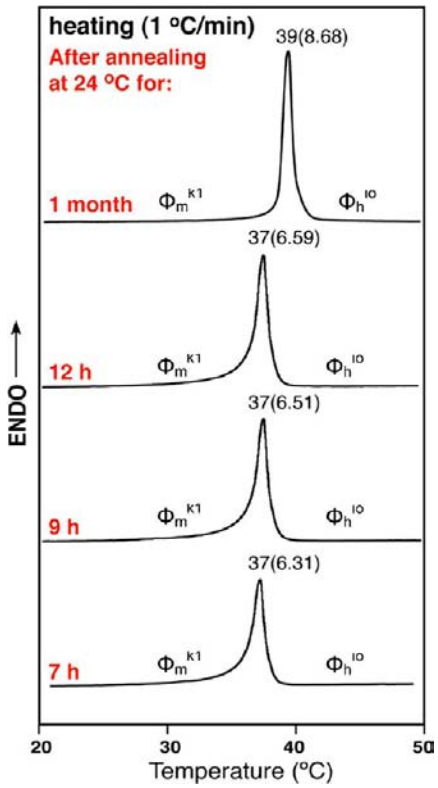

Figure 3. DSC heating traces (1 °C/min) for (3,4,5)12G1-1-PBI after annealing at room temperature for 7 h, 9 h, 12 h, and 1 month and cooling to the starting temperature at 1 °C/min.

The Φ_h^{io} phase disappears for compounds with n = 6 and 7 because the primary structure is too rigid to have the required conformational freedom for a 2D Φ_h^{io} liquid crystalline phase below the isotropic temperature. For all compounds, Φ_m^{k} is the thermodynamic product at the temperatures close to room temperature (24 °C).

The X-ray analysis shows that, at high temperature, compounds with n = 8 to 12 display a 2D Φ_h^{io} liquid crystalline columnar hexagonal phase with intracolumnar order (Tables 2 and ST1).

As expected, the column diameter of these supramolecular structures increases with the length of alkyl chains, n, of the tapered dendron. The supramolecular columns forming the Φ_h^{io} phase are constructed by a statistical mixture of the two arrangements shown in Figure 5g resulting in an all up/all down, and up−down alternation. The alternative up−down conformation acts as structural defects that disrupt the helical packing and generate the weak 7.0 Å diffraction in the meridional plot from Figure 5f. The 3.5 Å $\pi-\pi$ stacking between PBI planes generates the intracolumnar order with a correlation length that spans in average 34 column strata. The experimental density values and XRD data (Tables 2, ST1) were used to ascertain that the supramolecular columns have only one molecule per 3.5 Å thick stratum. The apparently meridional 7.0 Å diffraction (L = 2, or L = 6 in $\Phi_m^{k\text{-}SL}$ phase) is thought to be the result of the interdimer spacing, while the 3.5 Å diffraction (L = 4 or 12 in $\Phi_m^{k\text{-}SL}$ phase) comes from the intermolecular $\pi-\pi$ stacking of perylene planes (Figure 6). The $\pi-\pi$ stacking distance is conserved during the transition from the 2D to the 3D phases. It is apparent from Figure 6 that the 3D phases observed for n = 10, 9, 8, 7, 6 have a higher degree of order than those for n = 11, 12. This is particularly obvious from the appearance of sharp off-meridional diffraction arcs at increasing Bragg angles as n decreases. This indicates decreasing thermal disorder (Debye−Waller factor), understandable as the insulating alkyl sheath separating the columns is diminished.

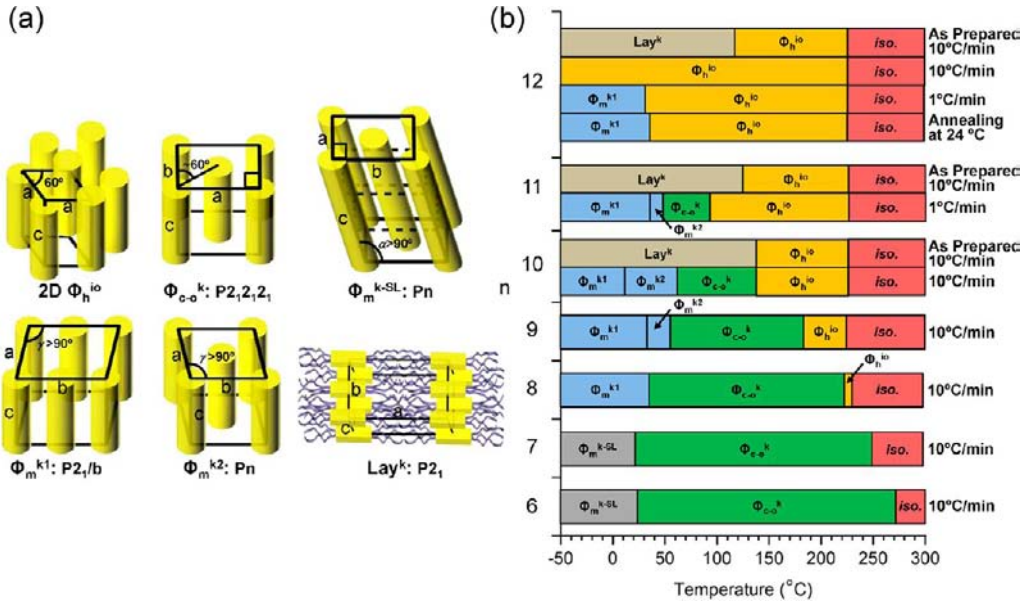

Figure 4. Schematic illustration of 2D and 3D periodic arrays self-organized from the supramolecular columns assembled from (3,4,5)nG1-1-PBI with n = 6 to 12. (a) Column arrangement of supramolecular columns in 2D and 3D lattices; their unit cell axis and angles are indicated. Phase notation: Φ_h^{io} , 2D columnar hexagonal phase with short-range intracolumnar order; $\Phi_{c\text{-}o}^{k}$, 3D columnar center orthorhombic lattice; $\Phi_m^{k\text{-}SL}$, 3D columnar monoclinic crystalline superlattice; Φ_m^{k1}, Φ_m^{k2}, 3D columnar crystalline monoclinic phases; Lay^k, layered monoclinic crystalline phase. (b) Dependence of the nature of 2D and 3D periodic arrays self-organized from (3,4,5)nG1-1-PBI as a function of n and temperature. Data were obtained from a combination of DSC and fiber and powder XRD analyses at the indicated heating rate.

dx.doi.org/10.1021/ja400639q | J. Am. Chem. Soc. 2013, 135, 4129−4148

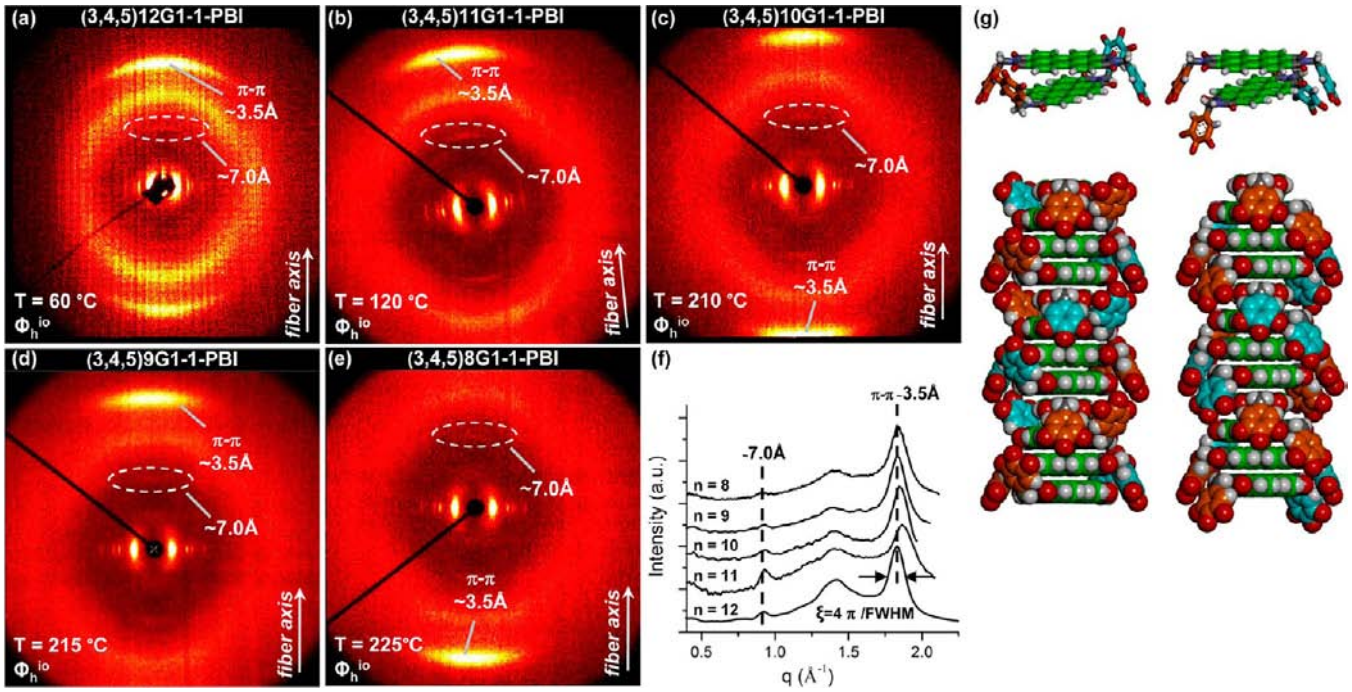

Figure 5. (a–e) Wide-angle XRD patterns collected from oriented fibers of (3,4,5)*n*G1-1-PBI with n = 8, 9, 10, 11, 12 in the 2D Φ_h^{io} phase at the temperature shown on the diffraction patterns. Fiber axis, temperature, phase designation, and $\pi-\pi$ stacking features are indicated. (f) The corresponding meridional plots from diffraction patterns shown in a–e. The correlation length (ξ) is calculated as 4π/fwhm, where fwhm corresponds to full width at half-maximum. (g) The two possible models of the supramolecular column. Color code: O atoms, red; H atoms, white; N atoms, blue; C atoms of the PBI, green; C atoms of the dendron phenyl, orange and light blue; all other atoms, gray.

Simulation of SAXS and WAXS Fiber Patterns. The ordered 2D and 3D phases reported in Figures 1–3 and Tables 1, 2, and ST1 were determined by the X-ray analysis recorded at both wide and small angles. XRD patterns for powder samples and oriented fibers extruded at room and higher temperatures were recorded as a function of temperature. The detailed experimental method for ther preparation of oriented fibers is reported in Supporting Figure SF1. The heating and cooling rates of these XRD experiments was kept in the range between 1 and 10 °C/min in order to match the experimental conditions used in the DSC experiments. The heating and cooling rates indicate the rate used to reach the required temperature. After reaching the required temperature with these rates the XRD pattern was recorded isothermally with an exposure time of 600 s.

The SAXS fiber patterns for n = 11, 10 and their indexing for the 3D ordered phases Φ_m^{k1}, Φ_m^{k2}, and $\Phi_{c\text{-}o}^{k}$ are shown in Figure 7. The supramolecular column of the Φ_m^{k1} phase is the thermodynamic product of the (3,4,5)*n*G1-1-PBI dendronized PBIs with n = 8 to 12. The same phase was studied previously for (3,4,5)12G1-1-PBI, revealing a criss-cross-like packing of dendronized PBIs within the supramolecular column possessing 2_1 helical symmetry.[13a] At low temperature, the formation of Φ_m^{k1} phase is under kinetic control for n = 12 and 11, and thermodynamic control for n = 10, 9, 8. It is the stable phase close to room temperature for compounds with n = 12 to 8. The intermediate crystalline phases between Φ_m^{k1} and Φ_h^{io} for n = 11 and 10 are Φ_m^{k2} and $\Phi_{c\text{-}o}^{k}$ as seen in Figure 7b,c for n = 11, and Figure 7e,f for n = 10. It can be seen from the SAXS pattern that the diffractions along the equator of $\Phi_{c\text{-}o}^{k}$ are similar to those observed in the Φ_h^{io} phase (Figure 5), indicating similar column arrangement within unit cell. Detailed XRD analysis combined with experimental density revealed an orthorhombic lattice, $\Phi_{c\text{-}o}^{k}$, with two columns in the unit cell possessing opposite helical chirality. The columns are constructed by stacking of supramolecular dimers along the *c*-axis.

For n = 10, the angle between two neighbor columns in the $\Phi_{c\text{-}o}^{k}$ phase is 60.4° (indicated in Figure 4a). This value is slightly deviated from that of a hexagonal lattice where the angle is 60° and therefore, this phase is a pseudo-hexagonal phase. The 7.0 Å (L = 2) diffraction remains in the intermediate $\Phi_{c\text{-}o}^{k}$ phase, which indicates that the $\pi-\pi$ stacking (3.5 Å) and the interdimer stacking distance is preserved and transferred from the 3D ordered phase to the 2D Φ_h^{io} phase. It can be concluded that as n increases, the intermediate crystalline structure transforms more and more toward hexagonal packing, and finally disappears for n = 12, where only one crystalline structure, Φ_m^{k1}, can be identified through a kinetically controlled process at low temperature.

Another crystalline phase observed in n = 11, 10, and 9 is Φ_m^{k2}, which is an intermediary phase connecting Φ_m^{k1} and $\Phi_{c\text{-}o}^{k}$. It is obtained during heating from the Φ_m^{k1} phase (Figure 2). The formation of Φ_m^{k2} is kinetically controlled in n = 11, and thermodynamically controlled in n = 10 and 9. The absence of (100) and (010) diffractions implies a monoclinic unit cell with cell symmetry of *Pn* that contains two columns in the unit cell with one column located in the cell center. Combination with experimental density suggests that the dimer packing is preserved in the Φ_m^{k2} phase. This makes the column arrangement similar with that of $\Phi_{c\text{-}o}^{k}$, but the unit cell is distorted in the *ab* plane ($\gamma > 90°$). It can be seen from the DSC traces that the transition from Φ_m^{k1} to Φ_m^{k2} is associated with a larger enthalpy change (3–6 kcal/mol), and the transition from Φ_m^{k2} to $\Phi_{c\text{-}o}^{k}$ is associated with a smaller enthalpy change (<1 kcal/mol). This suggests that the

dx.doi.org/10.1021/ja400639q | J. Am. Chem. Soc. 2013, 135, 4129–4148

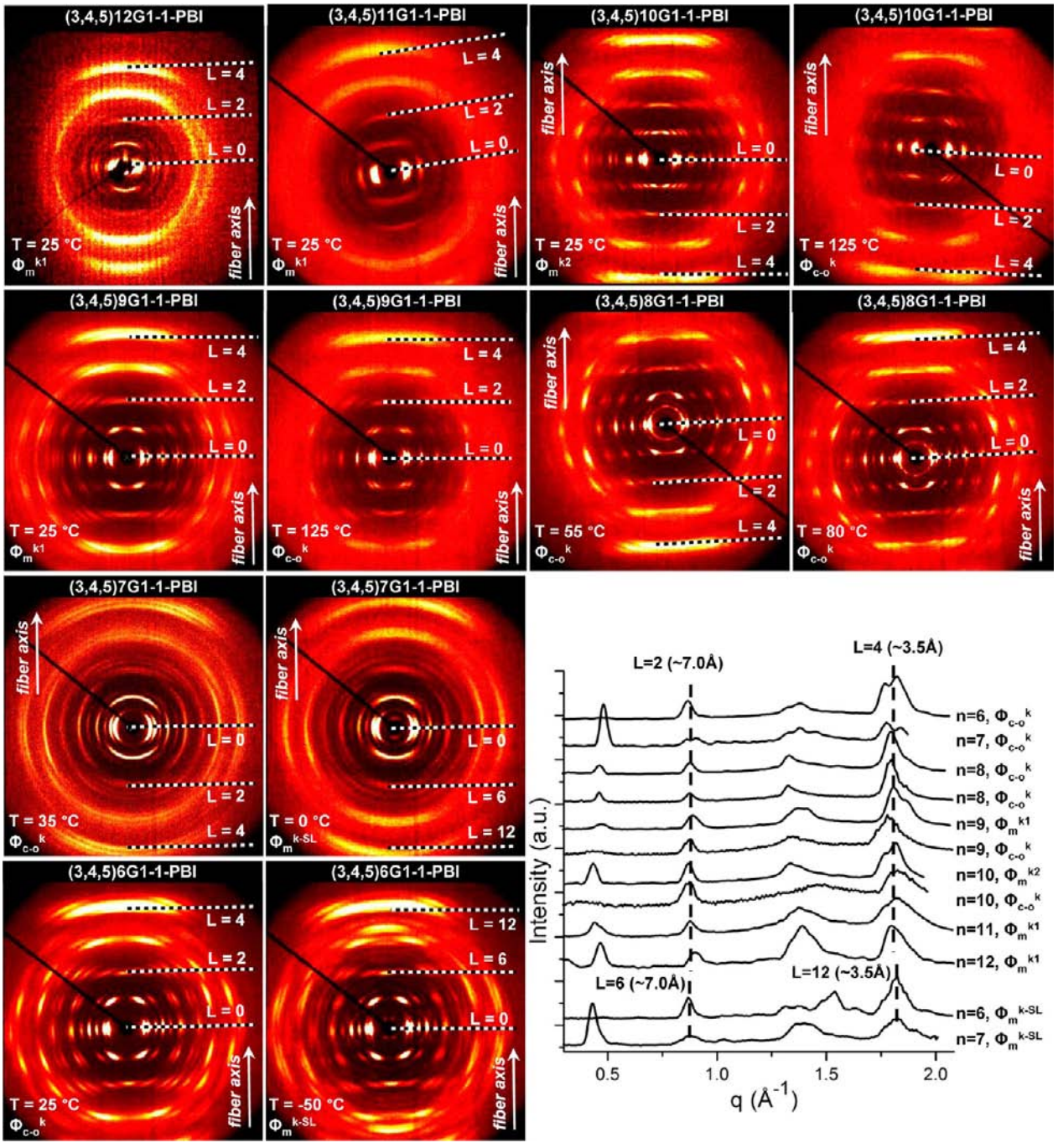

Figure 6. Wide-angle XRD patterns collected from the oriented fibers of (3,4,5)*n*G1-1-PBI with n = 6 to 12 in the 3D periodic arrays, and the corresponding meridional plots. For n = 12 the pattern was obtained after 180 min of annealing at 24 °C. For n = 11 the pattern was recorded during the second heating with a rate of 1 °C/min. Patterns for the other compounds were obtained during the second heating with a rate of 10 °C/min. Fiber axis, temperature, phase, and layer lines are indicated.

structural difference between Φ_m^{k1} and Φ_m^{k2} is larger than that between Φ_m^{k2} and $\Phi_{c\text{-}o}^{k}$. Also, the diffraction patterns of all three crystalline phases possess the same layer line distance, which implies the same number of strata along the *c*-axis and the same $\pi-\pi$ stacking distance between the PBI units.

Figure 8 shows the small-angle XRD patterns collected from the oriented fiber of (3,4,5)9G1-1-PBI and (3,4,5)8G1-1-PBI during second heating at a rate of 10 °C/min. The figure reveals the evolution of ordered phases observed in the two compounds as a function of increasing temperature.

By comparison with compounds with longer alkyl chain that were discussed above, a similar phase behavior was observed in n = 9. However, the conformational freedom decreases with decreasing n, and therefore, in n = 9, the 2D Φ_h^{io} phase exists in a narrower temperature range (183−227 °C) than for n = 10 or 11 (Figures 1 and 4b). In other words, the stability of the 3D ordered phase observed in n = 9 has increased to 183 °C, and the supramolecular columns require more energy to get released from the coupling interactions with neighboring columns. At lower temperature, close to room temperature, the monoclinic phase, Φ_m^{k1}, was observed as the thermody-

dx.doi.org/10.1021/ja400639q | J. Am. Chem. Soc. 2013, 135, 4129−4148

Table 2. Structural Analysis of (3,4,5)*n*G1-1-PBI with *n* = 6 to 12 by XRD and Experimental Density

n	*T* (°C)	phase[a]	*a*, *b*, *c* (Å)[b]	*α*, *β*, *γ* (deg)[b]	D_{col} (Å)[c]	*t* (Å)[d]	*ρ*[e] (g/cm^3)	M_{wt}[f]	*n*[g]	*μ*[h]
6	45	$\Phi_{c\text{-}o}^{k}$	36.2, 27.4, 14.7[j]	90.0, 90.0, 90.0	22.7	3.5	1.10	1171.55	8	1
	15	$\Phi_{m}^{k\text{-}SL}$	35.1, 29.7, 44.1[j]	114.6, 90.0, 90.0	23.0	3.5			24	1
7	35	$\Phi_{c\text{-}o}^{k}$	36.5, 28.8, 14.7[j]	90.0, 90.0, 90.0	23.2	3.5	1.09	1255.71	8	1
	0	$\Phi_{m}^{k\text{-}SL}$	35.8, 30.4, 44.1[j]	111.3, 90.0, 90.0	23.5	3.5			24	1
8	225	Φ_{h}^{io}	28.2, 28.2, –	–, –, 120.0	29.3	3.5	1.08	1339.86	–	1
	80	$\Phi_{c\text{-}o}^{k}$	37.6, 30.5, 14.5[j]	90.0, 90.0, 90.0	24.2	3.5			8	1
	55	$\Phi_{c\text{-}o}^{k}$	37.5, 30.9, 14.2[j]	90.0, 90.0, 90.0	23.9	3.5			8	1
	35	Φ_{m}^{k1}	24.5, 47.6, 14.2[j]	90.0, 90.0, 97.2	24.5	3.5			8	1
9	215	Φ_{h}^{io}	29.3, 29.3, –	–, –, 120.0	29.3	3.5	1.06	1424.02	–	1
	178	$\Phi_{c\text{-}o}^{k}$	41.7, 30.8, 14.2[j]	90.0, 90.0, 90.0	25.9	3.5			8	1
	125	$\Phi_{c\text{-}o}^{k}$	40.5, 30.8, 14.3[j]	90.0, 90.0, 90.0	25.4	3.5			8	1
	45	Φ_{m}^{k2}	32.0, 37.9, 14.3[j]	90.0, 90.0, 93.6	24.8	3.5			8	1
	25	Φ_{m}^{k1}	25.8, 47.3, 14.2[j]	90.0, 90.0, 96.8	25.8	3.5			8	1
	100	$\Phi_{c\text{-}o}^{ki}$	40.7, 30.6, 14.3[j]	90.0, 90.0, 90.0	25.5	3.5			8	1
10	210	Φ_{h}^{io}	29.8, 29.8, –	–, –, 120.0	30.2	3.5	1.04	1508.18	–	1
	125	$\Phi_{c\text{-}o}^{k}$	46.8, 30.6, 14.5[j]	90.0, 90.0, 90.0	27.9	3.5			8	1
	57	Φ_{m}^{k2}	34.8, 40.9, 14.3[j]	90.0, 90.0, 96.2	26.9	3.5			8	1
	25	Φ_{m}^{k2}	35.1, 40.0, 14.3[j]	90.0, 90.0, 97.1	26.6	3.5			8	1
	−35	Φ_{m}^{k1}	26.2, 47.2, 14.0[j]	90.0, 90.0, 96.3	26.2	3.5			8	1
	30	Lay^{ki}	43.9, 24.8, 4.6[j]	90.0, 115.0, 90.0	–	4.6			2	–
	110	Lay^{ki}	41.2, 25.0, 4.8[j]	90.0, 112.2, 90.0	–	4.8			2	–
11	120	Φ_{h}^{io}	30.2, 30.2, –	–, –, 120.0	30.2	3.5	1.03	1592.34	–	1
	75	$\Phi_{c\text{-}o}^{k}$	46.8, 30.9, 14.3[j]	90.0, 90.0, 90.0	29.0	3.5			8	1
	45	Φ_{m}^{k2}	35.5, 41.2, 14.5[j]	90.0, 90.0, 98.5	28.2	3.5			8	1
	25	Φ_{m}^{k1}	30.6, 47.3, 14.1[j]	90.0, 90.0, 94.2	30.6	3.5			8	1
	100	Lay^{ki}	45.8, 25.2, 4.7[j]	90.0, 116.0, 90.0	–	4.7			2	–
12	140	Φ_{h}^{io}	31.7, 31.7, –	–, –, 120.0	31.7	3.5	1.02	1676.50	–	1
	25	Φ_{m}^{k1}	32.5, 46.9, 14.2[j]	90.0, 90.0, 91.8	32.5	3.5			8	1
	−40	Φ_{m}^{k1}	32.1, 47.8, 14.0[j]	90.0, 90.0, 94.7	32.1	3.5			8	1
	−15	Lay^{ki}	51.1, 23.2, 4.8[j]	90.0, 115.0, 90.0	–	4.8			2	–
	20	Lay^{ki}	51.7, 24.6, 4.8[j]	90.0, 116.5, 90.0	–	4.8			2	–
	60	Lay^{ki}	47.6, 24.8, 4.8[j]	90.0, 113.5, 90.0	–	4.8			2	–

[a]Phase notation: Φ_h^{io}, 2D columnar hexagonal phase with intracolumnar order; $\Phi_{c\text{-}o}^{k}$, columnar centered orthorhombic crystalline phase; $\Phi_m^{k\text{-}SL}$, columnar monoclinic crystalline superlattice; Φ_m^{k}, columnar monoclinic crystalline phase; Lay^{k}, layered monoclinic crystalline phase. [b]Lattice parameters determined from fiber and powder XRDs. [c]Column diameter calculated using: $D_{col} = a$ for Φ_h^{io}, and $D_{col} = a/[2\cos(\tan^{-1} b/a)]$ for crystalline phases. [d]Stratum thickness calculated from the meriodional pattern. [e]Experimental density measured at 20 °C. [f]Molecular weight of the compound. [g]Average number of molecules per unit cell, calculated using $n = N_A \rho V_c/M_{wt}$, where $N_A = 6.022 \times 10^{23}$ mol^{-1} is the Avogadro's number, and V_c is the unit cell volume calculated from lattice parameters. [h]Average number of dendrimers forming the supramolecular column stratum, calculated using $\mu = N_A \rho A t/2M_{wt}$, where A is the unit cell area of the ab plane, and t is the average strata thickness calculated from the meriodional pattern. [i]Phase observed in as-prepared samples. [j]Fiber direction.

namic product that is generated independent of rate. Upon heating to 33 °C, a transition from Φ_m^{k1} to Φ_m^{k2} was observed with a transition enthalpy of 3.56 kcal/mol. Similar to the case of *n* = 11 and 10, this phase does not form upon cooling from the isotropic melt. The $\Phi_{c\text{-}o}^{k}$ phase in *n* = 9 exists upon heating regardless of rate at temperature above 55 °C. As in (3,4,5) *n*G1-1-PBI with *n* = 11 and 10, all phases in (3,4,5)9G1-1-PBI exhibit meridional maxima at 3.5 and 7.0 Å at *L* = 4 and 2, respectively. These features along with the experimental density (1.06 g/cm^3) confirm the formation of a supramolecular dimer structure.

SAXS fiber patterns of 3D and 2D ordered phases observed in (3,4,5)8G1-1-PBI during second heating with 10 °C/min are shown in Figure 8. The 2D Φ_h^{io} phase is generated from uncorrelated helical columns without intercolumnar order, as evidenced by the lack of quadrant diffractions (Figure 8f), while the 3D phases observed at low temperature are generated from coupled helical columns. These patterns demonstrate again that the transition between ordered phases in *n* = 8 is thermodynamically controlled and the column-to-column correlations developed without slow cooling or annealing at high temperature. At low temperature, Φ_m^{k1} is the stable phase as in the other compounds with *n* = 12 to 9. Upon heating to 37 °C (Figure 1), the Φ_m^{k1} transforms to $\Phi_{c\text{-}o}^{k}$ directly with a transition enthalpy of 6.04 kcal/mol without the intermediary Φ_m^{k2} phase. Also, the $\Phi_{c\text{-}o}^{k}$ phase with $P2_12_12_1$ symmetry in (3,4,5)8G1-1-PBI is found within a wider temperature range, 60−223 °C. This suggests that $\Phi_{c\text{-}o}^{k}$ becomes a more stable phase with decreasing *n* within the intermediary temperature range. In fact, for compounds with *n* = 7 and 6, the same $\Phi_{c\text{-}o}^{k}$ phase dominates the 3D ordered structure in an even wider temperature range, from close to room temperature up to over 250 °C. Their diffraction patterns will be discussed later. In addition, the temperature range of the 2D Φ_h^{io} phase from *n* = 8 is compressed to between 223 °C and the isotropization transition at 229 °C as a result of further decrease of the conformational freedom with the decrease of *n*. In other words, the stability of the long-range intra- and intercolumnar correlations is gradually increased by the decreased liquid-like

dx.doi.org/10.1021/ja400639q | J. Am. Chem. Soc. 2013, 135, 4129−4148

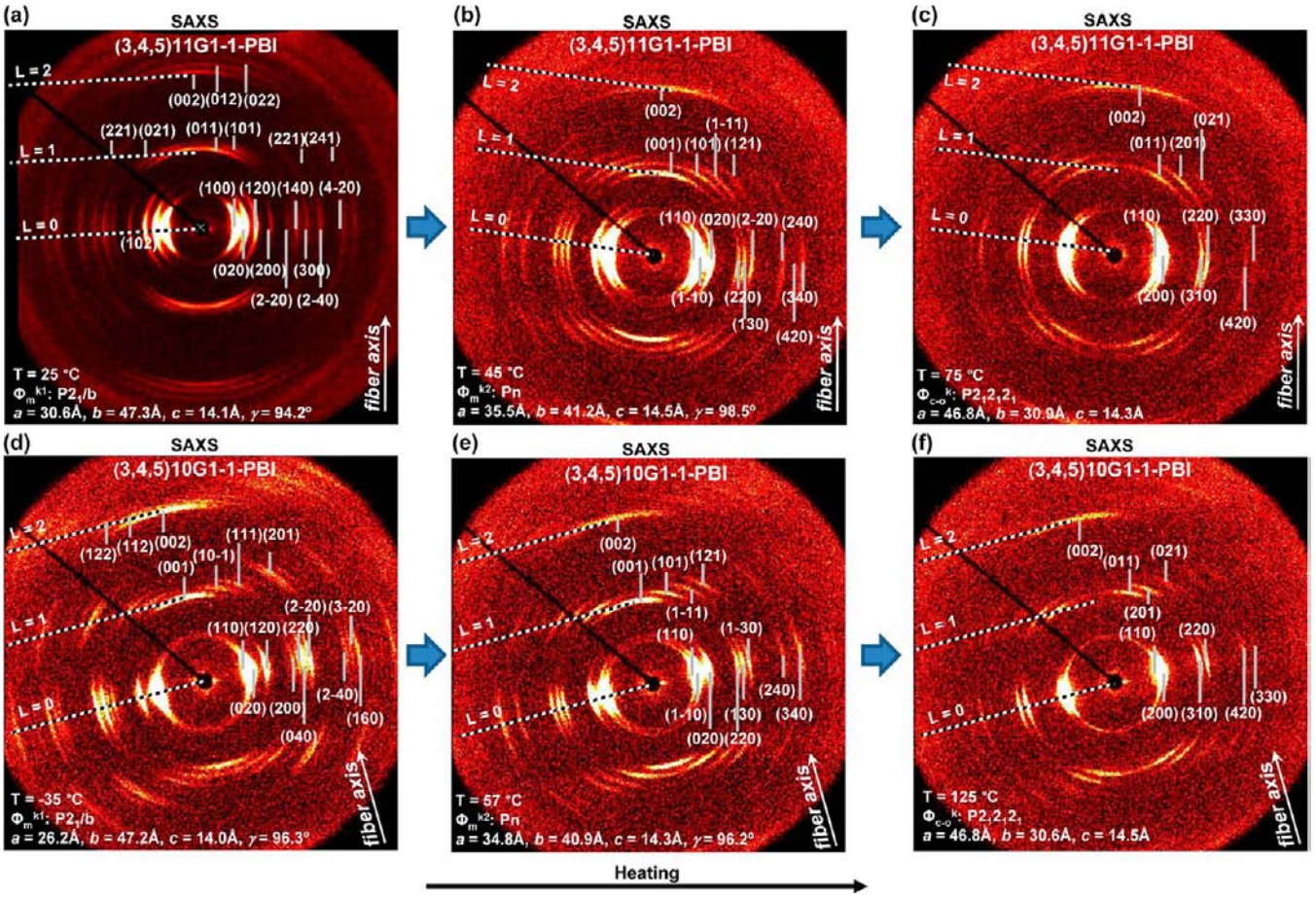

Figure 7. Small-angle XRD patterns collected from an oriented fiber of (3,4,5)11G1-1-PBI (a–c) and (3,4,5)10G1-1-PBI (d–f) showing 3D ordered phase at various temperatures during heating. Fiber axis, lattice symmetry, indexing, and lattice parameters of the Φ_m^{k1}, Φ_m^{k2}, and $\Phi_{c\text{-}o}^{k}$ phases are indicated. Patterns collected during second heating with a rate of 1 °C/min for n = 11 and 10 °C/min for n = 10.

character of the aliphatic jacket. The 2D Φ_h^{io} phase disappears when the length of alkyl chain is smaller than 8 (Figure 1, 2).

Figure 9a–c summarizes the comparison of experimental and simulated wide-angle fiber XRD patterns of (3,4,5)nG1-1-PBI with n = 9, 10, 11 in the Φ_m^{k1} phase with $P2_1/b$ symmetry. The detailed initial supramolecular column and lattice model in top and side views used for the simulation are shown in Figure 9d–f.

To conduct the XRD simulation, the energy-minimized primary molecular structure was first constructed by a combination of software packages including Materials Studio Modeling software (version 3.1.0) and Discovery Studio (version 3.5). The preliminary supramolecular columnar model was then constructed according to the helical parameter obtained from the XRD data. To build the crystal cell, the lattice dimension and symmetry group were extracted from the analysis of the primary XRD data by Datasqueeze (version 2.8), followed by unit cell construction in Materials Studio. The initial arrangement of supramolecular columns within the unit cell was judged by the lattice dimension, unit cell symmetry, and experimental density. Energy minimization was then performed to the unit cell to generate the initial model for XRD simulation. The initial unit cell model was exported to Accelrys Cerius2 (version 3.8), where the simulation of fiber XRD diffraction was performed. To produce the final model, minor model modifications in Cerius2 including inter- and intradimer rotation, supramolecular column rotation, and translation were performed until the simulated pattern fit best to the experimental XRD pattern. For the clarity of the core packing of dendronized PBIs, the tapered alkyl chains on both ends of the molecule are not shown in the unit cell models presented in all figures. A detailed flowchart of the phase determination and simulation process is summarized in Supporting Figure SF2.

As seen from the model shown in Figure 9, the column repeat c-axis is formed by stacking four molecules at 3.5 Å spacing. The dendronized PBIs are shifted inside the supramolecular column within the ab plane to avoid intracolumnar steric constrains. This off-centered molecule arrangement along the column axis shown in Figure 9d generates the 2_1 helical symmetry by rotation of molecule pairs by 180° along the c-axis. Each pair is constructed by two molecules forming a dimer-like repeating unit with an intradimer rotation around 80°. As shown in the side view of Figure 9f, along the b-axis lie alternate rows of supramolecular columns with respectively left- and right-handed helices that results from the $P2_1/b$ symmetry. The reconstructed relative electron density distributions of the Φ_m^{k1} phase in Figure 9g reveal the strong coupling of helical supramolecular columns in the low-temperature thermodynamic product. The difference in the diffraction patterns between compounds results from subtle variation of inter- and intradimer rotation and also the shift of dendronized PBIs in the supramolecular column with respect to the column center. It is apparent that the Φ_m^{k1} phase observed in n = 11 possesses

dx.doi.org/10.1021/ja400639q | J. Am. Chem. Soc. 2013, 135, 4129–4148

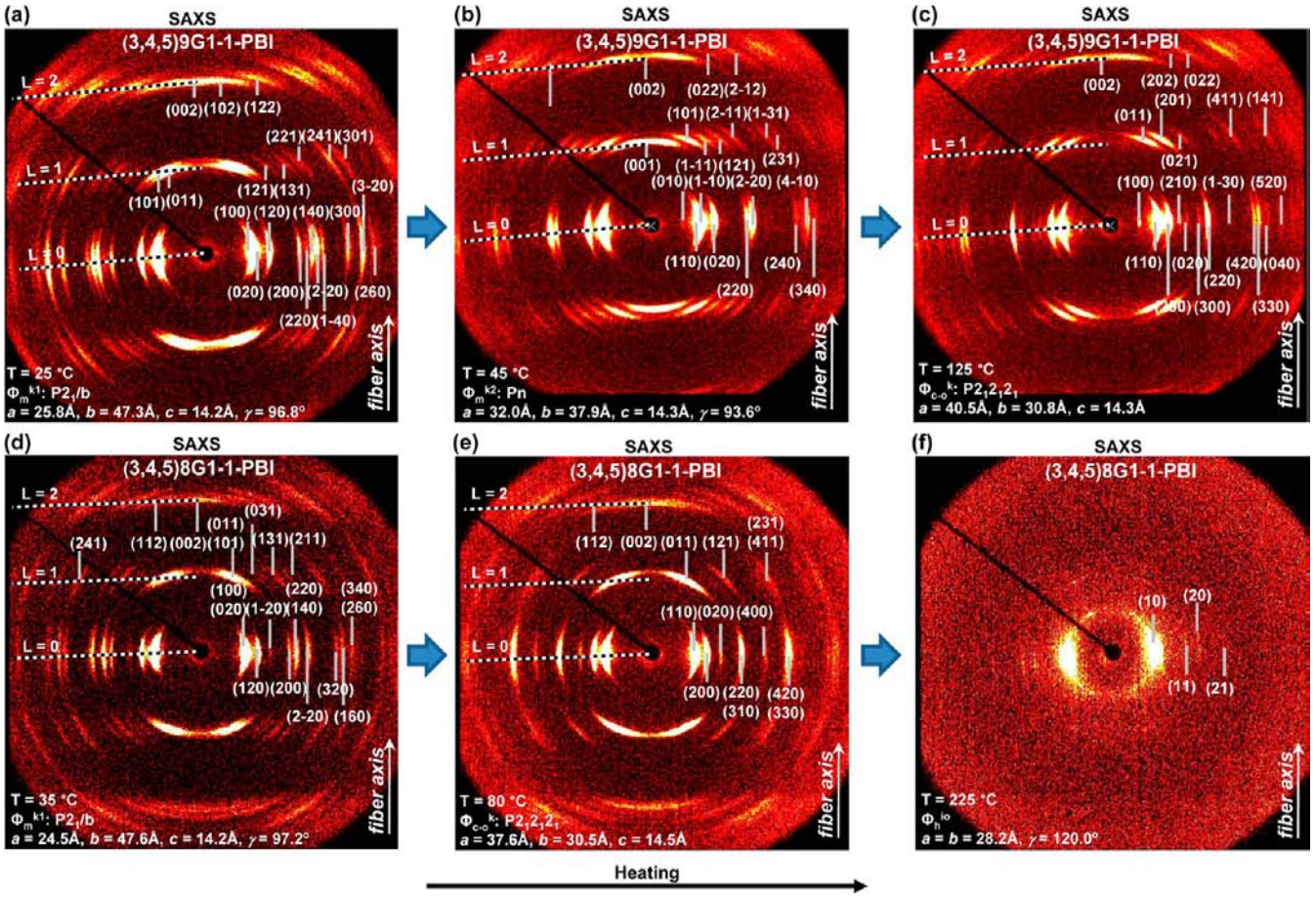

Figure 8. Small-angle XRD pattern collected from the oriented fibers of (3,4,5)9G1-1-PBI (a–c) and (3,4,5)8G1-1-PBI (d–f) during second heating with a rate of 10 °C/min, showing the observed 3D crystalline and 2D Φ_h^{io} phases at indicated temperatures. Fiber axis, symmetry, indexing, and lattice parameters of the corresponding phases are indicated.

a much lower order compared with that in n = 10 and 9, even though the pattern of n = 11 was collected during very slow cooling with a rate of 1 °C/min while the other two patterns were collected with a rate of 10 °C/min. Compared with the high-temperature 2D hexagonal and 3D orthorhombic arrays, the 3.5 Å stacking distance is conserved in Φ_m^{k1}, but the dendronized PBIs undergo significant changes with respect to their helical arrangement and centering within the column. These differences in packing and changes in ordering are responsible for the slower kinetics and larger enthalpy change observed in the formation of the Φ_m^{k1} phase.

Figure 10 details the lattice model in the $\Phi_{c\text{-}o}^{k}$ phase with $P2_12_12_1$ symmetry and a selected example showing the comparison between experimental and simulated fiber WAXS pattern for (3,4,5)8G1-1-PBI at 55 °C. The strong L = 4 meridional diffraction suggests that the column repeat c contains four molecules spaced at 3.5 Å. The repeat distance along c is about 14 Å, indicating that the columns in $\Phi_{c\text{-}o}^{k}$ have close to 8_1 helical symmetry. This is illustrated in Figure 10b. It can be clearly identified according to Figure 10c from the top view that the column packing is similar to that found in hexagonal arrays. Compared with the 2D hexagonal arrays obtained at high temperature, where the supramolecular columns possess no correlation with each other, the 3D intercolumn correlation developed during the transition from Φ_h^{io} to $\Phi_{c\text{-}o}^{k}$. In the 2D-to-3D transition, the columns are difficult to pack into a 3D hexagonal lattice since the symmetry would require a single column in one unit cell with all columns in the crystal having identical right- or left-handed helical arrangements. This is unlikely since this library of dendronized PBIs contains no chiral center that could control the chirality in the crystal. Therefore, the columns packed into an orthorhombic unit cell containing two columns with opposite chirality. The 2_1 symmetry operation in the orthorhombic cell would generate right- and left-handed columns in alternative rows (Figure 10c) and make the overall crystal achiral. The resulting column position in the unit cell is similar but deviates slightly from that in hexagonal arrays.

The undulated nature of the aromatic–aliphatic interface can also be identified in the 3D reconstructed electron density distribution. Figure 10d shows how the coupling of undulated columns produces the 3D column-to-column correlations. To construct the supramolecular column along the c-axis, a pair of molecules forming a dimer-like structure as repeat unit with the perylene planes stacked parallel but rotated ~45°. Two dimers generated the helical symmetry via ~90° rotation with respect to each other. The helical rotation along the c-axis is illustrated in Figure 10b, where a pair of molecules in the dimer are marked as red and blue, respectively. The sharp 7.0 Å meridional diffraction ((002) in Figure 8) is the result of the interdimer packing and persists through the whole temperature range below the isotropic state. The 3.5 Å π–π distance is conserved in a wide temperature range and displays long-range order.

dx.doi.org/10.1021/ja400639q | J. Am. Chem. Soc. 2013, 135, 4129–4148

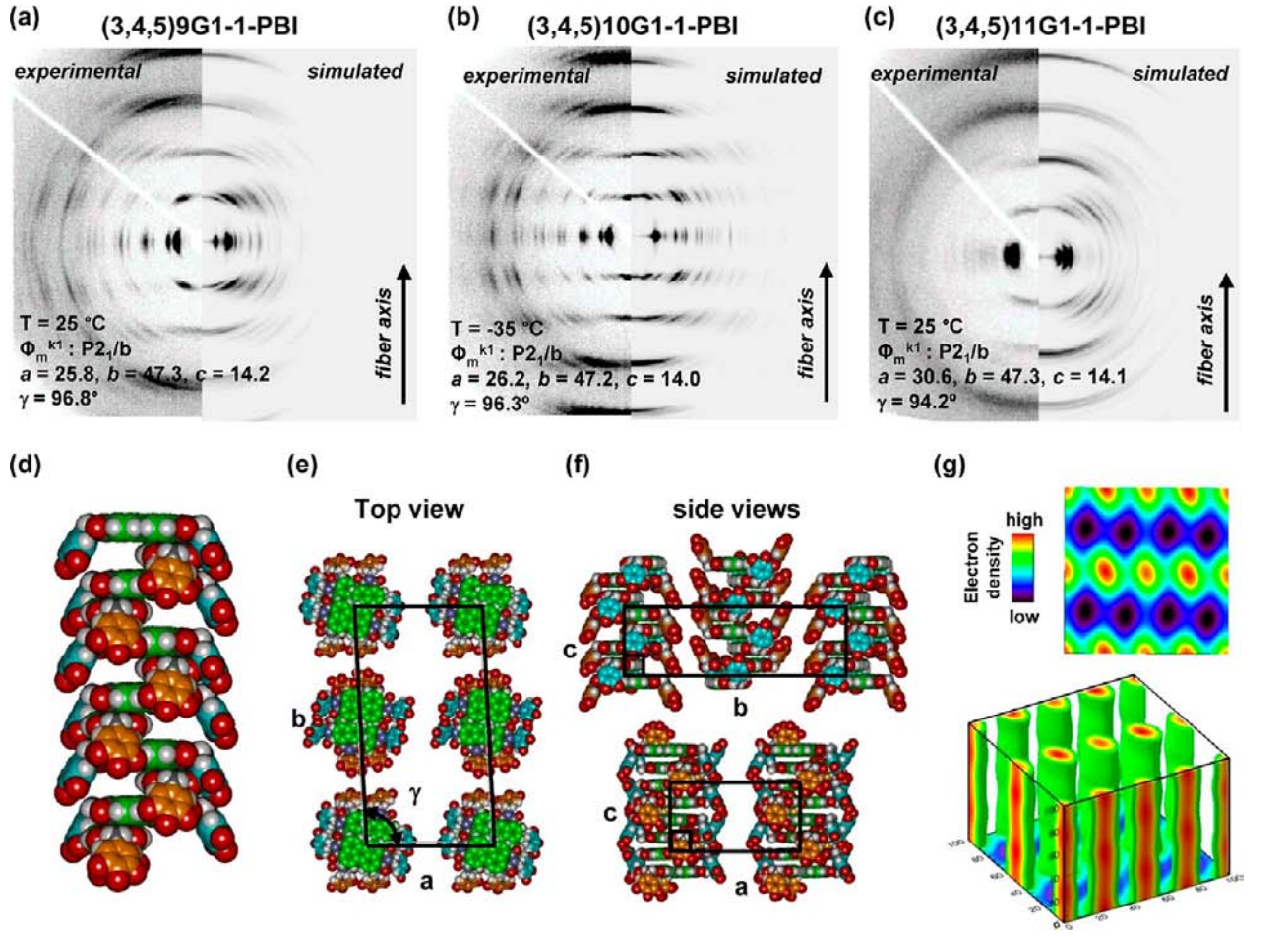

Figure 9. Comparison of the simulated and experimental WAXS fiber patterns of (3,4,5)*n*G1-1-PBI with *n* = 9 (a), 10 (b), 11 (c) in the columnar monoclinic crystalline phase, Φ_m^{k1}, at 25 °C, −35 °C, and 25 °C, respectively. The corresponding supramolecular column (d), the lattice model in top and side views used as the initial model in the simulation (e,f), and the 2D and 3D reconstructed relative electron density distribution of Φ_m^{k1} are also shown (g). Color code used in molecular models is the same as in Figure 5.

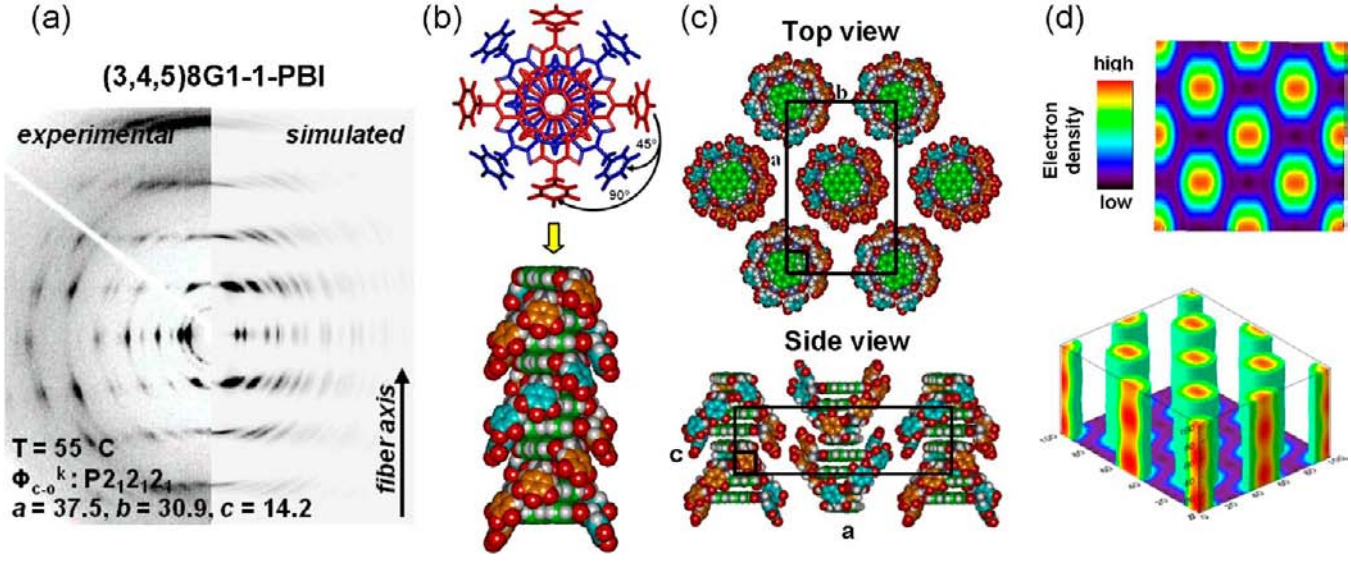

Figure 10. Comparison of the experimental and simulated wide-angle XRD patterns collected from the oriented fiber of (3,4,5)8G1-1-PBI at 55 °C in the columnar centered orthorhombic crystalline phase, $\Phi_{c\text{-}o}^{k}$ (a), and detail of the supramolecular column (b) and lattice model (c) used in the simulation. The 2D and 3D reconstructed relative electron density distributions are also shown (d). Color code used in the molecular model: O atoms, red; H atoms, white; N atoms, blue; C atoms of the PBI, green; C atoms of the dendron phenyl, orange and light blue; all other atoms, gray.

dx.doi.org/10.1021/ja400639q | *J. Am. Chem. Soc.* 2013, 135, 4129−4148

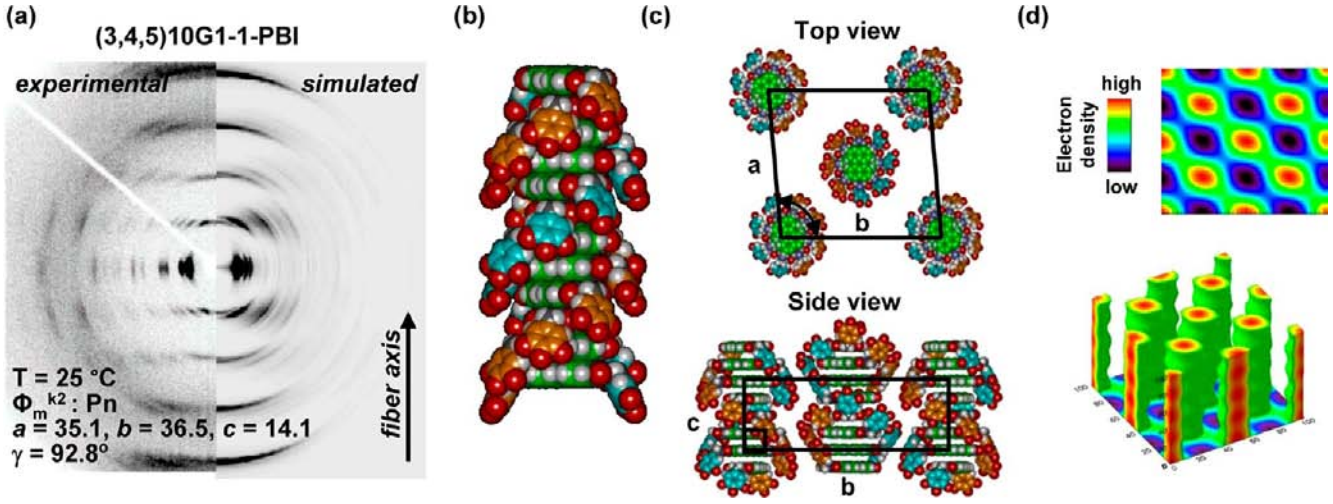

Figure 11. Comparison of the simulated and experimental fiber WAXS patterns of (3,4,5)10G1-1-PBI at 25 °C (a) in the columnar monoclinic crystalline phase, Φ_m^{k2}, and the corresponding supramolecular column (b) and lattice model in top and side views (c) used in the simulation. The 2D and 3D reconstructed relative electron density distributions are also shown (d). Color code used in the molecular model: O atoms, red; H atoms, white; N atoms, blue; C atoms of the PBI, green; C atoms of the dendron phenyl, orange and light blue; all other atoms, gray.

Figure 11 shows a selected example from (3,4,5)10G1-1-PBI that details the comparison between simulated and experimental fiber WAXS patterns of the Φ_m^{k2} phase with *Pn* symmetry collected at 25 °C. The molecular and column packing models used in the simulation are also illustrated (Figure 11b,c). This phase is observed during heating from the low-temperature stable Φ_m^{k1} phase in n = 11 to 9 before the columns transform into the $\Phi_{c\text{-}o}^{k}$. Judging from the intradimer (L = 4) and interdimer (L = 2) diffractions, the arrangement in Φ_m^{k2} is close to an 8_1 helix, with the neighbor PBI units separated by 3.5 Å. According to the symmetry operation, the columns located in the unit cell center possess different helical chirality than those located at corners. Although the stacking distance is conserved during the transition from Φ_m^{k1} to Φ_m^{k2}, the molecular rotation along the column axis and the 3D packing of columns within the unit cell are much different. This difference results in the slow kinetics observed for the formation of Φ_m^{k2} in n = 11.

As shown in Figure 11b, the column construction in Φ_m^{k2} shows helical symmetry similar to that found in $\Phi_{c\text{-}o}^{k}$, but the *ab* angle γ changes away from 90°. The small differences in the arrangement within the column and in the 3D packing of the supramolecular columns forming the 3D $\Phi_{c\text{-}o}^{k}$ and Φ_m^{k2} are responsible for the fast kinetics observed at the transition, and the associated enthalpy change is relatively small (for example, ΔH = 0.27 kcal/mol in n = 10, Figure 1). Combined with experimental density, the simulation reveals that, similar to the columns generated in other phases, the Φ_m^{k2} compound also forms columns via helical packing of only one molecule per stratum, with two columns in one unit cell. The 3D reconstructed electron density distributions shown in Figure 10d also illustrate the register between neighboring columns in the 3D Φ_m^{k2} crystalline phase. Notice that the column diameter (D_{col}) is nearly constant for all 3D phases generated by a single compound but gradually increases with increasing n (Table 2).

Figure 12 shows the SAXS patterns of the (3,4,5)6G1-1-PBI fiber extruded at 20 °C. The diffraction arcs with narrow azimuthal spread indicate that the supramolecular columns are easily aligned at room temperature. In the first heating of the as-prepared fiber, $\Phi_{c\text{-}o}^{k}$ is the only phase observed below the isotropization temperature at 272 °C. During the cooling scan, as shown in Figure 12, a transition from $\Phi_{c\text{-}o}^{k}$ to $\Phi_m^{k\text{-}SL}$ is identified at 27 °C (Figures 1, 2). Additional off-meridional diffractions were observed at L = 1 and 5 (Figure 12b, yellow arrow), indicating the tilt of the *c*-axis with respect to the *ab* plane. Also the appearance of additional layer lines indicates a tripling of the *c*-dimension of the cell compared with that of $\Phi_{c\text{-}o}^{k}$. The phase was indexed as monoclinic $\Phi_m^{k\text{-}SL}$, with *a* as the unique axis. The equatorial indices and spacings remain unchanged, indicating that the supramolecular column cross-section remains almost constant at the transition from the $\Phi_{c\text{-}o}^{k}$ to the $\Phi_m^{k\text{-}SL}$ lattice. The unit cell of $\Phi_m^{k\text{-}SL}$ contains three sub-cells along *c*, with a tilted *c*-axis of 14.7 Å. The same transition was observed at both 10 and 1 °C/min heating rates with almost identical transition temperature, suggesting that the transition is thermodynamically controlled, with a fast crystalline-to-crystalline rate near room temperature. Detailed XRD 2D patterns and 1D plots for n = 7 and 6 showing the peak intensities and the agreement between calculated and experimental *d*-spacings are in Supporting Figures SF8 and SF10.

In summary, four ordered phases were identified in the library of (3,4,5)*n*G1-1-PBI with n = 12 to 6, including one 2D Φ_h^{io} phase and three 3D crystalline phases (Φ_m^{k1}, Φ_m^{k2}, and $\Phi_{c\text{-}o}^{k}$) that are obtained by cooling from the isotropic melt or after annealing. Formation of the low-temperature 3D phases is under kinetic control for n = 12, 11 and thermodynamic control for n = 10 to 6, while formation of the 2D Φ_h^{io} phase at high temperature is under thermodynamic control for n = 12 to 8. The temperature range for the formation of Φ_h^{io} phase decreases as n decreases, and eventually disappears in compounds with n = 7 and 6. On the other hand, the stable temperature range for $\Phi_{c\text{-}o}^{k}$ phase increases with decreasing n. It is the stable 3D phase for a range of over 200 °C in n = 7 and 6, while it does not form at all in n = 12. At low temperature near room temperature, it seems that the stable phase is a monoclinic crystal for all compounds in this library. However, the larger difference with respect to intra- and intercolumn packing makes the phase slower to form and costs more energy. Interestingly, the as-prepared phase of n = 12, 11, and 10

dx.doi.org/10.1021/ja400639q | *J. Am. Chem. Soc.* 2013, 135, 4129−4148

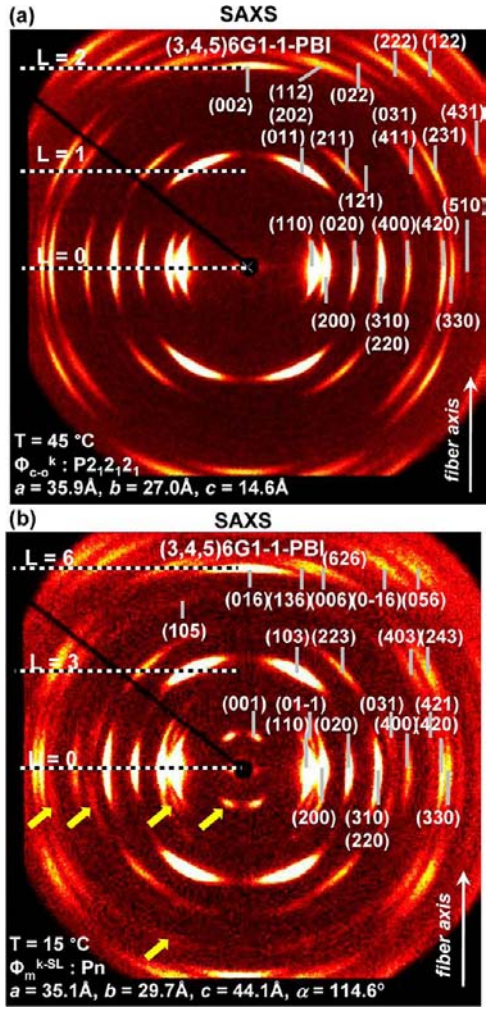

Figure 12. Small-angle XRD pattern collected from the oriented fiber of (3,4,5)6G1-1-PBI at (a) 45 and (b) 15 °C. Fiber axis, diffraction peaks, indexing, and lattice parameters of the columnar centered orthorhombic crystalline phase, $\Phi_{c\text{-}o}{}^{k}$, and columnar monoclinic crystalline superlattice, $\Phi_{m}{}^{k\text{-}SL}$, are indicated. Patterns collected during cooling with a rate of 10 °C/min. The extra diffractions that emerged at the $\Phi_{c\text{-}o}{}^{k}$-to-$\Phi_{m}{}^{k\text{-}SL}$ transition are indicated by yellow arrows in (b).

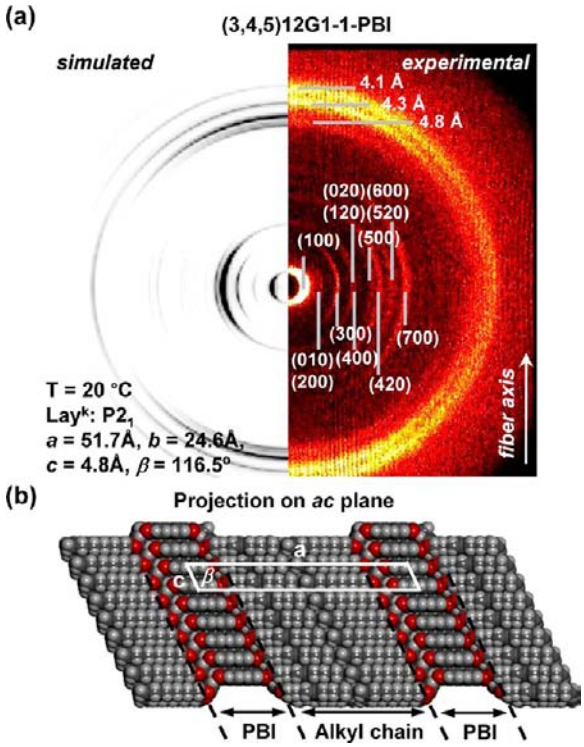

Figure 13. (a) Comparison of the experimental and simulated wide-angle XRD patterns collected from the oriented fiber of (3,4,5)12G1-1-PBI in the as-prepared condition, showing layered crystalline phase at 20 °C. Fiber axis, diffraction peaks, indexing, and lattice parameters are indicated. (b) Molecular model used in the simulation showing the construction of lamellar crystal and the layers of alkyl chain and PBI core.

obtained by slow evaporation of its THF or CH_2Cl_2 solution showed a completely different crystal structure that appears to be a layered crystal instead of a columnar crystal. This layered crystal structure is briefly discussed in the following session.

As-Prepared Phases of (3,4,5)12G1-1-PBI. The as-prepared sample refers to the compound purified repeatedly by column chromatography, dissolved in CH_2Cl_2, followed by solvent removal through slow evaporation (cast film), and dried overnight under vacuum. The as-prepared samples of (3,4,5) *n*G1-1-PBI with n = 12, 11, and 10 exhibit a layered crystalline structure in the first heating cycle that does not re-form in the subsequent heating and cooling experiments, and the transition from the layered crystal to 2D columnar arrays is associated with a large enthalpy change (Figures 1 and 2). This suggests that, inside the supramolecular structure, the PBI cores and alkyl tails are well phase-separated, and the long alkyl chains possess good packing with neighboring chains in the unit cell. These phases were investigated by powder and fiber XRD techniques. The oriented fibers were prepared by extrusion at 25 °C, with data shown in Figure 13 for n = 12, without performing any thermal treatment, from the as-prepared compounds. The detailed preparation method of oriented fibers is described in Supporting Figure SF1. Although the sample with layered structure (as-prepared from solvent evaporation) is crystalline, the alkyl chains still possess certain mobility at room temperature that makes the overall sample a highly viscous material. Therefore, it is possible to prepare oriented fibers by extrusion at room temperature of the sample with layered structure. During the extrusion, the alkyl chain layers can slide between each other and create the *c*-axis of the crystallites parallel to the fiber axis. The sample of n = 11 and 10 exhibits the same layered as-prepared structure as n = 12 (Supporting Information). Interestingly, this layered crystal is observed only in the as-prepared samples of n = 12 to 10. For n = 9 to 6, the layered structure does not form, and the as obtained samples show only 3D columnar structures. Figure 13a shows a comparison of experimental and simulated wide-angle XRD patterns of oriented fiber prepared from (3,4,5)12G1-1-PBI at 20 °C before any heat treatment. A 1D XRD plot showing the layered structure diffraction spacings is Supporting Figure SF6. The diffractions on the pattern equator fit nicely in a rectangular 2D lattice, indicating the γ angle is 90°. Taking the strongest meridional 4.3 Å peak as d_{001} and the 4.1 Å peak as d_{011} would suggest a monoclinic lattice with b as the unique axis. The weak diffraction on the meridian with spacing of 4.8 Å implies that β should be larger than 90°. According to the XRD pattern analysis and simulation combined with the experimental density, a monoclinic unit cell with $P2_1$ symmetry and parameters of a = 51.7 Å, b = 24.6

dx.doi.org/10.1021/ja400639q | J. Am. Chem. Soc. 2013, 135, 4129−4148

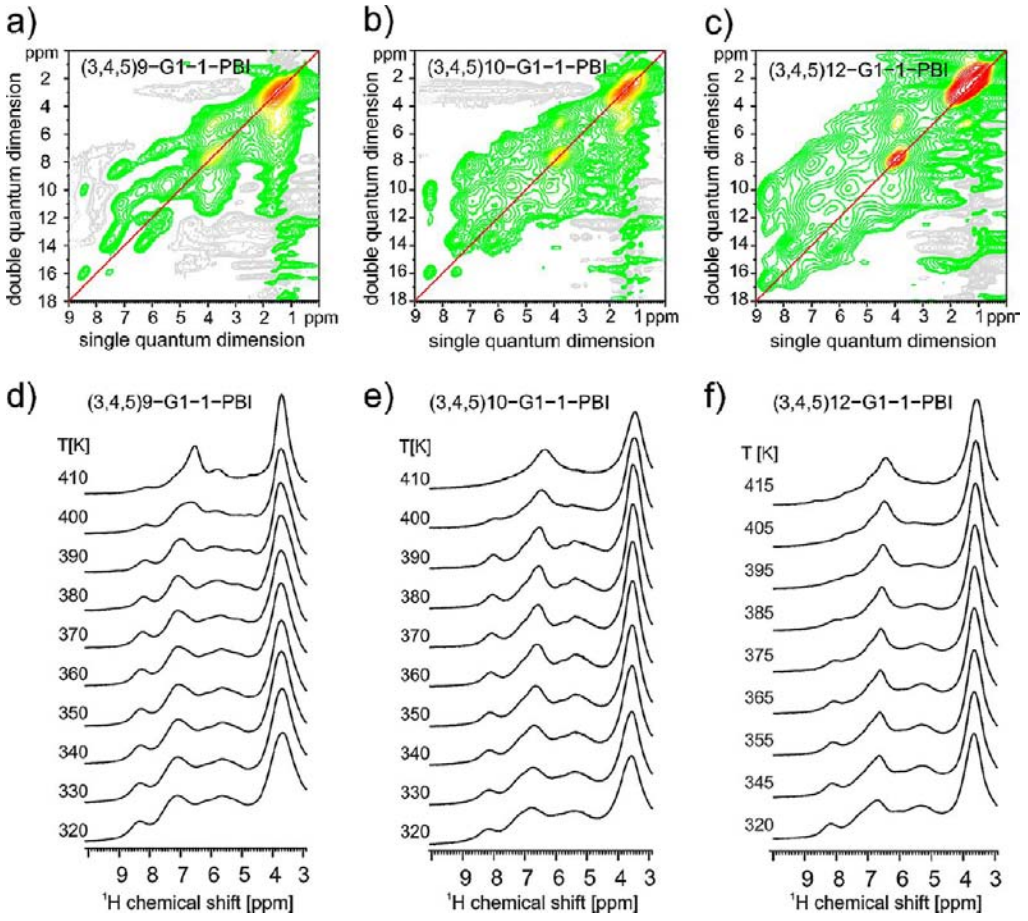

Figure 14. ^{1}H DQ correlation (a–c) and VT ^{1}H MAS (d–f) spectra of (a,d) (3,4,5)9-G1-1-PBI, (b,e) (3,4,5)10-G1-1-PBI, and (c,f) (3,4,5)12-G1-1-PBI. The well-defined ^{1}H sites of the thermodynamically controlled columnar monoclinic structure of (3,4,5)9-G1-1-PBI (a) provides a significantly better defined double-quantum correlation pattern compared to the slightly obscured double-quantum correlation pattern observed in the spectrum of the kinetically controlled monoclinic structure of (3,4,5)12-G1-1-PBI (c).

Å, c = 4.8 Å, and β = 116.5° is determined where each unit cell contains two molecules. The molecular model used in the simulation is shown in Figure 13b. In the model, the layered feature can be clearly identified. The PBI long axis and the alkyl chain direction are parallel to the unit cell a-axis, and the PBI planes are tilted with respect to the c-axis. In the XRD of layered crystals, the 3.5 Å π–π stacking diffraction that was found in other columnar phases is absent. According to this model, the stacking distance has increased to about 4.3 Å. This suggests that the distance between PBI planes is not optimized in this structure, and therefore, performance in terms of charge mobility would not be good compared with the columnar structures obtained after heating and annealing. We speculate that the formation of the layered crystal is probably a sacrifice to allow good packing of the long alkyl chains. With the decreasing of alkyl chain length, the tails would no longer have the power to keep the perylenes apart, and the stable columnar phases generated in the as-prepared sample with perylenes stack at 3.5 Å for n smaller than 10. Recently, functionalized PBI derivatives equipped with hydrogen-bonding units were reported to have a similar phase transition between a 2D supramolecular columnar structure and a layered structure.[16] However, opposite to the dendronized PBIs reported here, the columnar hexagonal phase was observed in the as-prepared sample of PBIs obtained by solvent casting. A structural transition to a highly ordered layered structure was observed during subsequent heating. Two previous reports published in 2004 and 2005 did not observe the layered structure reported here for (3,4,5)12G1-1-PBI.[8g,9c] This is most likely because the as-obtained sample was prepared by precipitation instead of evaporation, which suppressed the formation of well-ordered lamellar structure.

Analysis of the Molecular Dynamics of the Supramolecular Columns of (3,4,5)*n*G1-1-PBI with *n* = 9 and 10 by Variable-Temperature Solid-State ^{1}H NMR Experiments. In the solid state, NMR chemical shifts and in particular ^{1}H chemical shifts are very sensitive to the local molecular packing. Due to the substantial signal broadening resulting from anisotropic NMR interactions as well as the low spread of ^{1}H chemical shifts, NMR measurements at high magnetic fields and fast magic angle spinning (ω_R > 25 kHz) are required. Under these conditions, the spectral resolution obtained for chemically and crystallographically distinguished ^{1}H sites is limited by the local packing accuracy determining the electron density distribution at the site. In the case of materials based on self-organizing supramolecular architectures, minor variations of the local electron density at a specific packing site cause signal broadening, indicating the quality of the molecular self-organization. When the molecular packing arrangements of self-organizing systems are thermodynamically controlled with typically well-defined crystallographic sites, well-resolved, informative ^{1}H double-quantum correlation spectra are

dx.doi.org/10.1021/ja400639q | J. Am. Chem. Soc. 2013, 135, 4129–4148

Scheme 3. Schematic of the Self-Assembly of Dendronized PBIs (3,4,5)*n*G1-*m*-PBI with *m* = 0, 1, 2, 3, 4 and *n* = 14 to 4

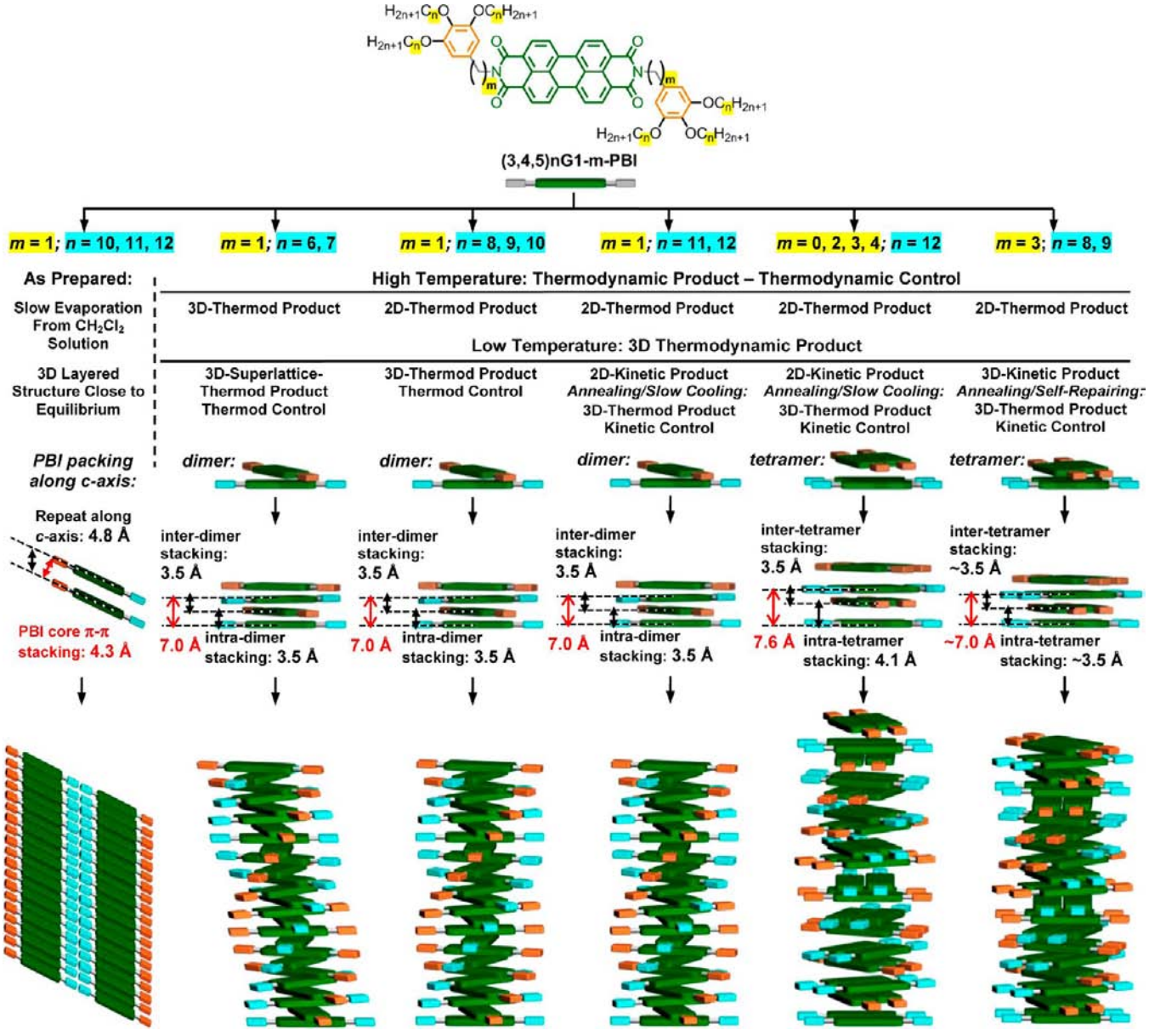

observed with common double-quantum recoupling schemes under fast MAS conditions. In contrast, ^{1}H NMR spectra of samples with kinetically controlled self-organization, which typically leads to a significantly higher molecular disorder in the material, exhibit substantially broader signals and in most cases a very poor spectral resolution. This low spectral resolution cannot be improved by the application of faster MAS, advanced homonuclear decoupling schemes, or even higher magnetic fields, since it is limited by the heterogeneous distribution of ^{1}H sites in the locally only partially ordered material.[17]

This is illustrated by the double-quantum correlation spectra given in Figure 14, in which the same correlation pattern of the columnar monoclinic phase shows a significantly lower spectral resolution for the aromatic signals of the PBI cores in (3,4,5)10-G1-1-PBI (Figure 14b) compared to those of the thermodynamically controlled columnar monoclinic phase of sample (3,4,5)9-G1-1-PBI shown in Figure 14a. Moreover, the spectral resolution in Figure 14b is significantly better compared to the correlation spectra of the kinetically controlled (3,4,5)12-G1-1-PBI sample shown in Figure 14c, where the aromatic signals are broadened so much that the identical underlying correlation pattern of the columnar monoclinic structure is hardly recognized.

In conventional ^{1}H VT MAS NMR measurements, the spectra of kinetically controlled (3,4,5)12-G1-1-PBI (see Figure 14f) show a smooth gradual transition from the low-temperature spectrum of the columnar monoclinic structure, common to all three samples at 320 K, to the spectrum of the hexagonal columnar meso-phase, characterized by a single broad proton signal in the aromatic region at 6.5 ppm. The same transition is observed in the ^{1}H VT MAS spectra of sample (3,4,5)10-G1-1-PBI shown in Figure 14e in a much narrower temperature range between 380 and 410 K. For the spectra of sample (3,4,5)9-G1-1-PBI shown in Figure 14d, the transition is not observed. The spectrum at 410 K, the highest temperature accessible to our 2.5 mm MAS probe, indicates some changes compared to the spectra at lower temperatures, which seem to be almost temperature independent. This

dx.doi.org/10.1021/ja400639q | J. Am. Chem. Soc. 2013, 135, 4129−4148

spectrum clearly deviates from the ^{1}H MAS NMR spectra of the two other samples at 410 K, with the single broad peak at 6.5 ppm attributed to the columnar hexagonal phase. From the DSC and X-ray studies shown before, the transition from the columnar orthorhombic to the columnar hexagonal phase is expected at 455 K. It should be noted that phase transitions being driven by molecular fluctuations or changing the local molecular mobility of specific sites in supramolecular architectures are not necessarily observed at the same temperature like in DSC traces, because most changes monitored in NMR spectra resulting from molecular mobility are sensitive to reorientations with a correlation time in the 100 kHz range which may not match the dynamic process driving or activated by the phase transition. In conclusion, the solid-state NMR results are nicely consistent with the experimental finding shown before, and thus confirm the transition from kinetically controlled to thermodynamically controlled columnar structures.

■ CONCLUSIONS

The results reported here, combined with those obtained in the two previous publications,[13a,b] are summarized in Scheme 3. This scheme, although simplified, demonstrates the complexity of the self-assembly of PBI containing self-assembling twin dendrons at its imide positions. All (3,4,5)*n*G1-*m*-PBI with m = 1 and n = 12 to 6 self-assemble into dimers forming 2D and 3D periodicities shown in the second to fourth columns from the left of Scheme 3. In the case of m = 0, 2, 3, 4 and $n \leq 12$, the dendronized PBI self-assembles in complex helical columns based on tetramers of PBI units comprising two columnar strata, two molecules lying side-by-side in each stratum. The distances and rotation angle within and between the tetramer strata are different. Exceptions are m = 3, n = 8 and 9, where a self-repairing process results in the intratetramer and intertetramer distances being equal. All compounds with m = 0, 2, 3, 4 exhibit at high temperature a 2D thermodynamic product that is thermodynamically controlled and at low temperature 3D thermodynamic products that are kinetically controlled. Therefore, under many conditions, at low temperature the 2D periodicity is observed as a kinetic product. This is illustrated in the first two columns on the right in Scheme 3. Also, at high temperature in the 2D Φ_h^{io} phase, the supramolecular columns constructed by dimers and tetramers contain a statistical mixture of up and down molecular arrangements (Figure 5). The random molecular conformation in columns disrupts the helical packing and generates the weak diffraction at ~7.0 Å.[13a] For the low-temperature 3D periodic arrays, the architecture of the repeat unit from 2D phase is preserved for both dimers and tetramers, but the molecules in supramolecular columns possess an ordered up-and-down arrangement within columns and between columns.[13] For the orthorhombic periodicity observed in m = 0, 2, 3, 4, the supramolecular columns consist of tetramers with alternate up-and-down molecular conformations that generate different intra- and intertetramer stacking distances.[13] Compounds with m = 1 and n = 12, 11 behave in the same way as those with m = 0, 2, 3, 4 except that they form dimers rather than tetramers. All compounds with m = 1 display equal intra- and interdimer distances resulting from the all-up or all-down orientation of the dendron groups within a column. The uniform orientation and up−down alternation among neighboring *columns* allows close and extended $\pi-\pi$ stacking that may allow superior charge carrier mobility and efficient transport. Contrasting the arrangement of the m = 1 library is the disruptive up−down alternation of the tetramer *within a column* found for m = 0, 2, 3, 4. *However, the as-prepared structures resultin from m = 1, n = 12, 11, and 10 are 3D layered rather than 3D columnar and are not re-formed after heating and cooling (left column in Scheme 3). Although this structure may represent the equilibrium structure from solution, it may not be the best structure for potential applications due to non-optimized PBI core stacking distance and difficulties in alignment.* As in the case of m = 0, 2, 3, 4, the 2D thermodynamic product from high temperature for m = 1 and n = 12 and 11 is thermodynamically controlled and becomes the kinetic product at low temperature since the 3D thermodynamic product from low temperature is kinetically controlled. For m = 1 and n = 10, 9, 8 the 2D thermodynamic product that is thermodynamically controlled at high temperature transferred to the 3D thermodynamic product at low temperature regardless of cooling rate since the transition from 2D to 3D phase becomes thermodynamically controlled. For m = 1 and n = 7 and 6 the transitions between phases are all thermodynamically controlled (independent of rate), similar to those observed for m = 1 with n = 10 to 8. However, the 3D crystalline phases dominate the whole temperature range below isotropic temperature without a transition from 3D crystalline phase to 2D liquid crystalline phase. In addition, a new phase, $\Phi_m^{k\text{-}SL}$, is developed below room temperature, generated from tilted columns of $\Phi_{c\text{-}o}^{k}$, which is reminiscent of the self-repairing process observed from m = 3 and n = 9 and 8.[13b] The helical supramolecular columns forming 2D and 3D periodic arrays reported here are chiral, but the unit cell is nonracemic since it contains a left and a right helical column. However, it is also important to understand how the chirality of the chemical structure could affect the self-assembly and the kinetic and thermodynamic supramolecular products, and if homochirality could lead to any difference in the electronic properties of dendronized PBI. The investigation of chiral compounds will be discussed in a future publication. Last but not least, we would like to stress that most of the supramolecular assemblies reported in the literature are routinely based on structures involving *n*-dodecyl alkyl groups.[1−3,5,7−13,15] The results reported here demonstrate that shorter than eleven methylene groups in the self-assembling building block may be more suitable than *n*-dodecyl for all reported investigations; therefore, we recommend the use of a combination of lengths of alkyl groups in future investigations.

■ ASSOCIATED CONTENT

Ⓢ Supporting Information

Experimental procedures with complete spectral and structural analysis. This material is available free of charge via the Internet at http://pubs.acs.org.

■ AUTHOR INFORMATION

Corresponding Author

percec@sas.upenn.edu

Notes

The authors declare no competing financial interest.

■ ACKNOWLEDGMENTS

Financial support by the National Science Foundation (DMR-1066116, DMR-1120901, DMS-0935165, and OISE-1243313), the Humboldt Foundation, and the P. Roy Vagelos Chair at Penn is gratefully acknowledged. This work was also financially

supported by the German Research Foundation (DFG) through grant SFB 625, by the European FP7 Project NANOGOLD (grant 228455), and the WCU Program funded by the Ministry of Education, Science, and Technology of Korea (R31-10013).

REFERENCES

(1) (a) Ustinov, A.; Weissman, H.; Shirman, E.; Pinkas, I.; Zuo, X.; Rybtchinski, B. *J. Am. Chem. Soc.* **2011**, *133*, 16201−16211. (b) Iron, M. A.; Cohen, R.; Rybtchinski, B. *J. Phys. Chem. A* **2011**, *115*, 2047−2056. (c) Shao, C.; Grüne, M.; Stolte, M.; Würthner, F. *Chem.—Eur. J.* **2012**, *18*, 13665−13677. (d) Wasielewski, M. R. *Acc. Chem. Res.* **2009**, *42*, 1910−1921. (e) Sinks, L. E.; Rybtchinski, B.; Iimura, M.; Jones, B. A.; Goshe, A. J.; Zuo, X. B.; Tiede, D. M.; Li, X. Y.; Wasielewski, M. R. *Chem. Mater.* **2005**, *17*, 6295−6303. (f) Fuller, M. J.; Sinks, L. E.; Rybtehinski, B.; Giaimo, J. M.; Li, X. Y.; Wasielewski, M. R. *J. Phys. Chem. A* **2005**, *109*, 970−975. (g) Rosen, B. M.; Wilson, C. J.; Wilson, D. A.; Peterca, M.; Imam, M. R.; Percec, V. *Chem. Rev.* **2009**, *109*, 6275−6540. (h) Percec, V.; Aqad, E.; Peterca, M.; Imam, M. R.; Glodde, M.; Bera, T. K.; Miura, Y.; Balagurusamy, V. S. K.; Ewbank, P. C.; Würthner, F.; Heiney, P. A. *Chem.—Eur. J.* **2007**, *13*, 3330−3345.

(2) (a) Görl, D.; Zhang, X.; Würthner, F. *Angew. Chem., Int. Ed.* **2012**, *51*, 6328−6348. (b) Würthner, F.; Stolte, M. *Chem. Commun.* **2011**, *47*, 5109−5115. (c) Würthner, F.; Kaiser, T. E.; Saha-Möller, C. R. *Angew. Chem., Int. Ed.* **2011**, *50*, 3376−3410. (d) Huang, C.; Barlow, S.; Marder, S. R. *J. Org. Chem.* **2011**, *76*, 2386−2407. (e) Usta, H.; Facchetti, A.; Marks, T. J. *Acc. Chem. Res.* **2011**, *44*, 501−510. (f) Chen, Z.; Lohr, A.; Saha-Möller, C. R.; Würthner, F. *Chem. Soc. Rev.* **2009**, *38*, 564−584. (g) Würthner, F. *Chem. Commun.* **2004**, 1564−1579. (h) Langhals, H. *Heterocycles* **1995**, *40*, 477−500. (i) Ustinov, A.; Weissman, H.; Shirman, E.; Pinkas, I.; Zuo, X.; Rybtchinski, B. *J. Am. Chem. Soc.* **2011**, *133*, 16201−16211. (j) Rybtchinski, B. *ACSNano* **2011**, *5*, 6791−6818. (k) Weissman, H.; Rybtchinski, B. *Curr. Opin. Colloid Interface Sci.* **2012**, *17*, 330−342.

(3) (a) Yue, W.; Lv, A.; Gao, J.; Jiang, W.; Hao, L.; Li, C.; Li, Y.; Polander, L. E.; Barlow, S.; Hu, W.; Di Motta, S.; Negri, F.; Marder, S. R.; Wang, Z. *J. Am. Chem. Soc.* **2012**, *134*, 5770−5773. (b) Huang, C.; Sartin, M. M.; Cozzuol, M.; Siegel, N.; Barlow, S.; Perry, J. W.; Marder, S. R. *J. Phys. Chem. A* **2012**, *116*, 4305−4317. (c) Huang, C.; Potscavage, W. J., Jr.; Tiwari, S. P.; Sutcu, S.; Barlow, S.; Kippelen, B.; Marder, S. R. *Polym. Chem* **2012**, *3*, 2996−3006. (d) Zhan, X.; Facchetti, A.; Barlow, S.; Marks, T. J.; Ratner, M. A.; Wasielewski, M. R.; Marder, S. R. *Adv. Mater.* **2011**, *23*, 268−284. (e) Carsten, B.; He, F.; Son, H. J.; Xu, T.; Yu, L. *Chem. Rev.* **2011**, *111*, 1493−1528. (f) Weissman, H.; Ustinov, A.; Shimoni, E.; Cohen, S. R.; Rybtchinski, B. *Polym. Adv. Technol.* **2011**, *22*, 133−138. (g) Anthony, J. E.; Facchetti, A.; Heeney, M.; Marder, S. R.; Zhan, X. *Adv. Mater.* **2010**, *22*, 3876−3892. (h) Zhan, X.; Tan, Z. a.; Zhou, E.; Li, Y.; Misra, R.; Grant, A.; Domercq, B.; Zhang, X.-H.; An, Z.; Zhang, X.; Barlow, S.; Kippelen, B.; Marder, S. R. *J. Mater. Chem.* **2009**, *19*, 5794−5803. (i) Zhan, X.; Tan, Z. a.; Domercq, B.; An, Z.; Zhang, X.; Barlow, S.; Li, Y.; Zhu, D.; Kippelen, B.; Marder, S. R. *J. Am. Chem. Soc.* **2007**, *129*, 7246−7247. (j) Blanco, R.; Gomez, R.; Seoane, C.; Segura, J. L.; Mena-Osteritz, E.; Bauerle, P. *Org. Lett.* **2007**, *9*, 2171−2174. (k) Facchetti, A. *Chem. Mater.* **2011**, *23*, 733−758.

(4) *Supramolecular Dye Chemistry*; Würthner, F., Ed.; Topics in Current Chemistry 258; Springer-Verlag: Berlin, 2005. (b) *Color Chemistry*, 3rd ed.; Zollinger, H.; Wiley-VCH; Weinheim, 2003. (c) *Industrial Organic Pigments: Production, Properties, Applications*, 3rd ed.; Herbst, W.; Hunger, K.; Wiley-VCH: Meinheim, 2004. (d) Klebe, G.; Graser, F.; Hädicke, E.; Berndt, J. *Acta Crystallographica Section B-Structural Science* **1989**, *45*, 69−77. (e) Graser, F.; Hädicke, E. *Liebigs Ann. Chem.* **1980**, 1994−2011. (f) Graser, F.; Hädicke, E. *Liebigs Ann. Chem.* **1984**, 483−494.

(5) (a) Zang, L.; Liu, R. C.; Holman, M. W.; Nguyen, K. T.; Adams, D. M. *J. Am. Chem. Soc.* **2002**, *124*, 10640−10641. (b) Baumstark, D.; Wagenknecht, H.-A. *Angew. Chem., Int. Ed.* **2008**, *47*, 2612−2614. (c) Zhang, X.; Chen, Z.; Würthner, F. *J. Am. Chem. Soc.* **2007**, *129*, 4886−4887. (d) Zhang, X.; Rehm, S.; Safont-Sempere, M. M.; Würthner, F. *Nat. Chem.* **2009**, *1*, 623−629.

(6) Law, K. Y. *Chem. Rev.* **1993**, *93*, 449−486.

(7) (a) Qu, J. Q.; Pschirer, N. G.; Liu, D. J.; Stefan, A.; De Schryver, F. C.; Müllen, K. *Chem.—Eur. J.* **2004**, *10*, 528−537. (b) Cotlet, M.; Masuo, S.; Lor, M.; Fron, E.; Van der Auweraer, M.; Müllen, K.; Hofkens, J.; De Schryver, F. *Angew. Chem., Int. Ed.* **2004**, *43*, 6116−6120. (c) Kaiser, T. E.; Wang, H.; Stepanenko, V.; Würthner, F. *Angew. Chem., Int. Ed.* **2007**, *46*, 5541−5544. (d) Kaiser, T. E.; Stepanenko, V.; Würthner, F. *J. Am. Chem. Soc.* **2009**, *131*, 6719−6732.

(8) (a) Fischer, M. K. R.; Kaiser, T. E.; Würthner, F.; Baeuerle, P. *J. Mater. Chem.* **2009**, *19*, 1129−1141. (b) Backes, C.; Schmidt, C. D.; Hauke, F.; Boettcher, C.; Hirsch, A. *J. Am. Chem. Soc.* **2009**, *131*, 2172−2184. (c) Heek, T.; Fasting, C.; Rest, C.; Zhang, X.; Würthner, F.; Haag, R. *Chem. Commun.* **2010**, *46*, 1884−1886. (d) Schmidt, C. D.; Boettcher, C.; Hirsch, A. *Eur. J. Org. Chem.* **2009**, 5337−5349. (e) Backes, C.; Schmidt, C. D.; Rosenlehner, K.; Hauke, F.; Coleman, J. N.; Hirsch, A. *Adv. Mater.* **2010**, *22*, 788−802. (f) Würthner, F.; Thalacker, C.; Diele, S.; Tschierske, C. *Chem.—Eur. J.* **2001**, *7*, 2245−2253. (g) van Herrikhuyzen, J.; Syamakumari, A.; Schenning, A.; Meijer, E. W. *J. Am. Chem. Soc.* **2004**, *126*, 10021−10027. (h) Würthner, F.; Chen, Z. J.; Hoeben, F. J. M.; Osswald, P.; You, C. C.; Jonkheijm, P.; van Herrikhuyzen, J.; Schenning, A.; van der Schoot, P.; Meijer, E. W.; Beckers, E. H. A.; Meskers, S. C. J.; Janssen, R. A. J. *J. Am. Chem. Soc.* **2004**, *126*, 10611−10618. (i) Chen, Z.; Baumeister, U.; Tschierske, C.; Würthner, F. *Chem.—Eur. J.* **2007**, *13*, 450−465. (j) Würthner, F.; Chen, Z. J.; Dehm, V.; Stepanenko, V. *Chem. Commun.* **2006**, 1188−1190. (k) Chen, Z.; Stepanenko, V.; Dehm, V.; Prins, P.; Siebbeles, L. D. A.; Seibt, J.; Marquetand, P.; Engel, V.; Würthner, F. *Chem.—Eur. J.* **2007**, *13*, 436−449. (l) Debije, M. G.; Chen, Z. J.; Piris, J.; Neder, R. B.; Watson, M. M.; Müllen, K.; Würthner, F. *J. Mater. Chem.* **2005**, *15*, 1270−1276. (m) Li, X.-Q.; Stepanenko, V.; Chen, Z.; Prins, P.; Siebbeles, L. D. A.; Würthner, F. *Chem. Commun.* **2006**, 3871−3873. (n) Li, X.-Q.; Zhang, X.; Ghosh, S.; Würthner, F. *Chem.—Eur. J.* **2008**, *14*, 8074−8078.

(9) (a) Cormier, R. A.; Gregg, B. A. *J. Phys. Chem. B* **1997**, *101*, 11004−11006. (b) Cormier, R. A.; Gregg, B. A. *Chem. Mater.* **1998**, *10*, 1309−1319. (c) An, Z. S.; Yu, J. S.; Jones, S. C.; Barlow, S.; Yoo, S.; Domercq, B.; Prins, P.; Siebbeles, L. D. A.; Kippelen, B.; Marder, S. R. *Adv. Mater.* **2005**, *17*, 2580−2583. (d) Shoaee, S.; An, Z.; Zhang, X.; Barlow, S.; Marder, S. R.; Duffy, W.; Heeney, M.; McCulloch, I.; Durrant, J. R. *Chem. Commun.* **2009**, 5445−5447. (e) An, Z.; Yu, J.; Domercq, B.; Jones, S. C.; Barlow, S.; Kippelen, B.; Marder, S. R. *J. Mater. Chem.* **2009**, *19*, 6688−6698. (f) Dehm, V.; Chen, Z.; Baumeister, U.; Prins, P.; Siebbeles, L. D. A.; Würthner, F. *Org. Lett.* **2007**, *9*, 1085−1088. (g) Duzhko, V.; Aqad, E.; Imam, M. R.; Peterca, M.; Percec, V.; Singer, K. D. *Appl. Phys. Lett.* **2008**, *92*, 113312.

(10) (a) Hasenknopf, B.; Lehn, J. M.; Boumediene, N.; Leize, E.; Van Dorsselaer, A. *Angew. Chem., Int. Ed.* **1998**, *37*, 3265−3268. (b) Philp, D.; Stoddart, J. F. *Angew. Chem., Int. Ed.* **1996**, *35*, 1155−1196. (c) Kidd, T. J.; Leigh, D. A.; Wilson, A. J. *J. Am. Chem. Soc.* **1999**, *121*, 1599−1600. (d) Ashton, P. R.; Glink, P. T.; MartinezDiaz, M. V.; Stoddart, J. F.; White, A. J. P.; Williams, D. J. *Angew. Chem., Int. Ed.* **1996**, *35*, 1930−1933. (e) Lubrich, D.; Green, S. J.; Turberfield, A. J. *J. Am. Chem. Soc.* **2009**, *131*, 2422−2423. (f) Northrop, B. H.; Khan, S. J.; Stoddart, J. F. *Org. Lett.* **2006**, *8*, 2159−2162. (g) Nguyen, H. D.; Reddy, V. S.; Brooks, C. L. *Nano Lett.* **2007**, *7*, 338−344. (h) Cui, H.; Chen, Z.; Zhong, S.; Wooley, K. L.; Pochan, D. J. *Science* **2007**, *317*, 647−650.

(11) (a) Percec, V.; Cho, W. D.; Ungar, G.; Yeardley, D. J. P. *J. Am. Chem. Soc.* **2001**, *123*, 1302−1315. (b) Percec, V.; Mitchell, C. M.; Cho, W. D.; Uchida, S.; Glodde, M.; Ungar, G.; Zeng, X. B.; Liu, Y. S.; Balagurusamy, V. S. K.; Heiney, P. A. *J. Am. Chem. Soc.* **2004**, *126*, 6078−6094. (c) Percec, V.; Peterca, M.; Sienkowska, M. J.; Ilies, M. A.; Aqad, E.; Smidrkal, J.; Heiney, P. A. *J. Am. Chem. Soc.* **2006**, *128*, 3324−3334. (d) Percec, V.; Holerca, M. N.; Nummelin, S.; Morrison, J. L.; Glodde, M.; Smidrkal, J.; Peterca, M.; Rosen, B. M.; Uchida, S.;

Balagurusamy, V. S. K.; Sienkowska, M. L.; Heiney, P. A. *Chem.—Eur. J.* **2006**, *12*, 6216−6241. (e) Percec, V.; Won, B. C.; Peterca, M.; Heiney, P. A. *J. Am. Chem. Soc.* **2007**, *129*, 11265−11278. (f) Percec, V.; Peterca, M.; Dulcey, A. E.; Imam, M. R.; Hudson, S. D.; Nummelin, S.; Adelman, P.; Heiney, P. A. *J. Am. Chem. Soc.* **2008**, *130*, 13079−13094. (g) Percec, V.; Imam, M. R.; Peterca, M.; Wilson, D. A.; Heiney, P. A. *J. Am. Chem. Soc.* **2009**, *131*, 1294−1304. (h) Percec, V.; Imam, M. R.; Peterca, M.; Wilson, D. A.; Graf, R.; Spiess, H. W.; Balagurusamy, V. S. K.; Heiney, P. A. *J. Am. Chem. Soc.* **2009**, *131*, 7662−7677. (i) Percec, V.; Imam, M. R.; Peterca, M.; Cho, W.-D.; Heiney, P. A. *Isr. J. Chem.* **2009**, *49*, 55−70. (j) Peterca, M.; Imam, M. R.; Leowanawat, P.; Rosen, B. M.; Wilson, D. A.; Wilson, C. J.; Zeng, X.; Ungar, G.; Heiney, P. A.; Percec, V. *J. Am. Chem. Soc.* **2010**, *132*, 11288−11305. (k) Rosen, B. M.; Peterca, M.; Huang, C.; Zeng, X.; Ungar, G.; Percec, V. *Angew. Chem., Int. Ed.* **2010**, *49*, 7002−7005. (l) Percec, V.; Wilson, D. A.; Leowanawat, P.; Wilson, C. J.; Hughes, A. D.; Kaucher, M. S.; Hammer, D. A.; Levine, D. H.; Kim, A. J.; Bates, F. S.; Davis, K. P.; Lodge, T. P.; Klein, M. L.; DeVane, R. H.; Aqad, E.; Rosen, B. M.; Argintaru, A. O.; Sienkowska, M. J.; Rissanen, K.; Nummelin, S.; Ropponen, J. *Science* **2010**, *328*, 1009−1014. (m) Rosen, B. M.; Wilson, D. A.; Wilson, C. J.; Peterca, M.; Won, B. C.; Huang, C.; Lipski, L. R.; Zeng, X.; Ungar, G.; Heiney, P. A.; Percec, V. *J. Am. Chem. Soc.* **2009**, *131*, 17500−17521. (n) Tomalia, D. A. *J. Nanopart. Res.* **2009**, *11*, 1251−1310. (o) Tomalia, D. A. *Soft Matter* **2010**, *6*, 456−474. (p) Peterca, M.; Percec, V.; Leowanawat, P.; Bertin, A. *J. Am. Chem. Soc.* **2011**, *133*, 20507−20520.

(12) (a) Balagurusamy, V. S. K.; Ungar, G.; Percec, V.; Johansson, G. *J. Am. Chem. Soc.* **1997**, *119*, 1539−1555. (b) Hudson, S. D.; Jung, H. T.; Percec, V.; Cho, W. D.; Johansson, G.; Ungar, G.; Balagurusamy, V. S. K. *Science* **1997**, *278*, 449−452. (c) Percec, V.; Ahn, C. H.; Ungar, G.; Yeardley, D. J. P.; Möller, M.; Sheiko, S. S. *Nature* **1998**, *391*, 161−164. (d) Percec, V.; Cho, W. D.; Möller, M.; Prokhorova, S. A.; Ungar, G.; Yeardley, D. J. P. *J. Am. Chem. Soc.* **2000**, *122*, 4249−4250. (e) Yeardley, D. J. P.; Ungar, G.; Percec, V.; Holerca, M. N.; Johansson, G. *J. Am. Chem. Soc.* **2000**, *122*, 1684−1689. (f) Percec, V.; Glodde, M.; Bera, T. K.; Miura, Y.; Shiyanovskaya, I.; Singer, K. D.; Balagurusamy, V. S. K.; Heiney, P. A.; Schnell, I.; Rapp, A.; Spiess, H. W.; Hudson, S. D.; Duan, H. *Nature* **2002**, *419*, 384−387. (g) Ungar, G.; Liu, Y. S.; Zeng, X. B.; Percec, V.; Cho, W. D. *Science* **2003**, *299*, 1208−1211. (h) Percec, V.; Dulcey, A. E.; Balagurusamy, V. S. K.; Miura, Y.; Smidrkal, J.; Peterca, M.; Nummelin, S.; Edlund, U.; Hudson, S. D.; Heiney, P. A.; Hu, D. A.; Magonov, S. N.; Vinogradov, S. A. *Nature* **2004**, *430*, 764−768. (i) Zeng, X. B.; Ungar, G.; Liu, Y. S.; Percec, V.; Dulcey, S. E.; Hobbs, J. K. *Nature* **2004**, *428*, 157−160.

(13) (a) Percec, V.; Peterca, M.; Tadjiev, T.; Zeng, X.; Ungar, G.; Leowanawat, P.; Aqad, E.; Imam, M. R.; Rosen, B. M.; Akbey, U.; Graf, R.; Sekharan, S.; Sebastiani, D.; Spiess, H. W.; Heiney, P. A.; Hudson, S. D. *J. Am. Chem. Soc.* **2011**, *133*, 12197−12219. (b) Percec, V.; Hudson, S. D.; Peterca, M.; Leowanawat, P.; Aqad, E.; Graf, R.; Spiess, H. W.; Zeng, X.; Ungar, G.; Heiney, P. A. *J. Am. Chem. Soc.* **2011**, *133*, 18479−94.

(14) Percec, V.; Keller, A. *Macromolecules* **1990**, *23*, 4347−4350.

(15) (a) Ungar, G.; Abramic, D.; Percec, V.; Heck, J. A. *Liq. Cryst.* **1996**, *21*, 73−86. (b) Percec, V.; Ahn, C. H.; Bera, T. K.; Ungar, G.; Yeardley, D. J. P. *Chem.—Eur. J.* **1999**, *5*, 1070−1083. (c) Percec, V.; Bera, T. K.; Glodde, M.; Fu, Q. Y.; Balagurusamy, V. S. K.; Heiney, P. A. *Chem.—Eur. J.* **2003**, *9*, 921−935. (d) Percec, V.; Peterca, M.; Yurchenko, M. E.; Rudick, J. G.; Heiney, P. A. *Chem.—Eur. J.* **2008**, *14*, 909−918. (e) Percec, V.; Rudick, J. G.; Peterca, M.; Yurchenko, M. E.; Smidrkal, J.; Heiney, P. A. *Chem.—Eur. J.* **2008**, *14*, 3355−3362.

(16) Yagai, S.; Usui, M.; Seki, T.; Murayama, H.; Kikkawa, Y.; Uemura, S.; Karatsu, T.; Kitamura, A.; Asano, A.; Seki, S. *J. Am. Chem. Soc.* **2012**, *134*, 7983.

(17) (a) Brown, S. P. *Prog. Nucl. Magn. Reson. Spectrosc.* **2007**, *50*, 199−251. (b) Schmidt, J.; Hoffmann, A.; Spiess, H. W.; Sebastiani, D. *J. Phys. Chem. B* **2006**, *110*, 23204−23210. (c) Hansen, M. R.; Graf, R.; Sekharan, S.; Sebastiani, D. *J. Am. Chem. Soc.* **2009**, *131*, 5251−5256. (d) Dudenko, D.; Kiersnowski, A.; Shu, J.; Pisula, W.; Sebastiani, D.; Spiess, H. W.; Hansen, M. R. *Angew. Chem., Int. Ed.* **2012**, *51*, 11068−11072.